Inorganic Chemistry

pubs.acs.org/IC Article

Ruthenium(II) Phosphine/Mercapto Complexes: Their in Vitro Cytotoxicity Evaluation and Actions as Inhibitors of Topoisomerase and Proteasome Acting as Possible Triggers of Cell Death Induction

Gabriel H. Ribeiro,* Adriana P. M. Guedes, Tamires D. de Oliveira, Camila R. S. T. b. de Correia, Legna Colina-Vegas, Mauro A. Lima, Joaquim A. Nóbrega, Márcia R. Cominetti, Fillipe V. Rocha, Antônio G. Ferreira, Eduardo E. Castellano, Felipe R. Teixeira, and Alzir A. Batista*

Cite This: https://dx.doi.org/10.1021/acs.inorgchem.0c01835 Read Online

ACCESS | Metrics & More | Article Recommendations | Supporting Information

ABSTRACT: In this paper, a series of new ruthenium complexes of the general formula $[Ru(NS)(dpphpy)(dppb)]PF_6$ (**Ru1**−**Ru3**), where dpphpy = diphenyl-2-pyridylphosphine, NS ligands = 2-thiazoline-2-thiol (tzdt, **Ru1**), 2-mercaptopyrimidine (pySm, **Ru2**), and 4,6-diamino-2-mercaptopyrimidine (damp, **Ru3**), and dppb = 1,4-bis(diphenylphosphino)butane, were synthesized and characterized by elemental analysis, spectroscopic techniques (IR, UV/visible, and 1D and 2D NMR), and X-ray diffraction. In the characterization, the correlation between the phosphorus atoms and their respective aromatic hydrogen atoms of the compounds in the assignment stands outs, by $^{1}H-^{31}P$ HMBC experiments. The compounds show anticancer activities against A549 (lung) and MDA-MB-231 (breast) cancer cell lines, higher than the clinical drug cisplatin. All of the complexes are more cytotoxic against the cancer cell lines than against the MRC-5 (lung) and MCF-10A (breast) nontumorigenic human cell lines. For A549 tumor cells, cell cycle analysis upon treatment with **Ru2** showed that it inhibits the mitotic phase because arrest was observed in the Sub-G1 phase. Additionally, the compound induces cell death by an apoptotic pathway in a dose-dependent manner, according to annexin V-PE assay. The multitargeted character of the compounds was investigated, and the biomolecules were DNA, topoisomerase IB, and proteasome, as well as the fundamental biomolecule in the pharmacokinetics of drugs, human serum albumin. The experimental results indicate that the complexes do not target DNA in the cells. At low concentrations, the compounds showed the ability to partially inhibit the catalytic activity of topoisomerase IB in the process of relaxation of the DNA plasmid. Among the complexes assayed in cultured cells, complex **Ru3** was able to diminish the proteasomal chymotrypsin-like activity to a greater extent.

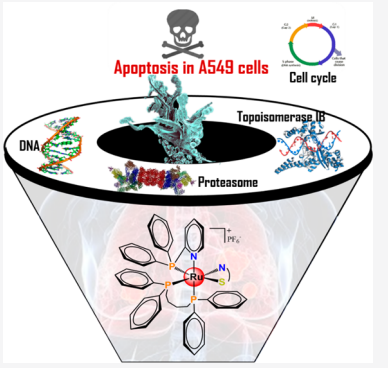

INTRODUCTION

Metallodrug chemotherapy represented by cisplatin and other platinum-based drugs have become the first line of anticancer treatment because of their significant antitumor efficacy.[1,2] Since platinum-based drugs were introduced in cancer treatment, a variety of potential novel metal-based chemotherapeutics have been investigated.[3,4] In this framework, the in vitro and in vivo antitumor activities of ruthenium compounds have proved to be notable, showing good selective bioactivity and the ability to overcome the resistance and side effects encountered in both organic and platinum-based anticancer drugs.[5−10] Thus, there are a large number of reports on inorganic complexes that have been investigated within the frame of a possible "ruthenotherapy".[11−13]

In this context, our research group has contributed to this field, developing new ruthenium(II) phosphine complexes containing different types of coligands aimed at the possibility of identifying synergisms of the metallic center and functional ligands.[14−18] Notably, ruthenium(II) diphosphine compounds containing derivatives of mercapto ligands (NS) have attracted our attention,[19−24] especially complexes of the general formula $[Ru(NS)(bipy)(dppb)]^{+}$[25] [dppb = 1,4-bis-(diphenylphosphino)butane; bipy = 2,2′-bipyridine] and $[Ru(NS)(PP)_2]^{+}$[26] [PP = 1,1′-bis(diphenylphosphino)-methane (dppm) and 1,2-bis(diphenylphosphino)ethane (dppe)]. In general, synthesized complexes have shown high, in vitro, cytotoxicity against several cancer cell lines and high selectivity for tumor cells. For example, the complex $[Ru(mmi)(bipy)(dppb)]PF_6$[19] (mmi = 2-mercapto-1-methyl-imidazole) showed potent cytotoxicity against cells HepG2 (human hepatocellular carcinoma), with the IC_{50} value of 2.6

Received: June 23, 2020

https://dx.doi.org/10.1021/acs.inorgchem.0c01835
Inorg. Chem. XXXX, XXX, XXX−XXX

± 0.8 μM. The complex showed good activity, in vivo, reducing the growth of HepG2 cells (human liver cancer cell line) that were engrafted in C.B-17 SCID mice. The animals treated with the [Ru(mmi)(bipy)(dppb)]PF_6 complex had tumor mass inhibition rates of 31.5−45.4% compared to the negative control.[19] In the same experiment, doxorubicin reduced the tumor weight by 36.8% compared to that of the negative control.[19]

In the present study, on the basis of the previous experience gained by our research group with ruthenium(II) complexes, three new complexes, [Ru(tzdt)(dpphpy)(dppb)]PF_6 (**Ru1**; CCDC 2006233), [Ru(pySm)(dpphpy)(dppb)]PF_6 (**Ru2**; CCDC 2006235), and [Ru(damp)(dpphpy)(dppb)]PF_6 (**Ru3**; CCDC 2006234) [dpphpy = diphenyl-2-pyridylphosphine, tzdt = 2-thiazoline-2-thiol, pySm = 2-mercaptopyrimidine, and damp = 4,6-diamino-2-mercaptopyrimidine], were synthesized and characterized. One of the inspirations for the design of these complexes was use of the ambidentate dphppy ligand,[27−30] associated with the dppb ligand, resulting in complexes with good hydrophobic properties.[31,32] Presumably, these features of the complexes can cause great uptake in cells and also a possible intensification of the interaction between compounds and biomolecules.[33−35] Herein, we also evaluate the capacity of the three compounds (**Ru1**, **Ru2**, and **Ru3**) to inhibit the proteasome activity. The ubiquitin proteasome system is a multicatalytic protease complex involved in the degradation of misfolded, damaged, or unneeded intracellular proteins.[36] In cancer cells, proteasomes are highly expressed and hyperactivated because of deregulation of their homeostatic function. Tumor suppressor proteins, which play a role in regulating cell division, inducing cell cycle arrest, are potential target proteins of the ubiquitin proteasome system.[37−41] In cancer therapy, some proteasome inhibitors are clinically useful for the treatment of some types of cancer.[42] Proteasome inhibitors regulate protein turnover and the accumulation of proteins engaged in cell cycle regulation. The proteasome inhibitors are able to activate cell cycle arrest and the apoptotic and autophagy death processes.

Here, interaction studies of human serum albumin (HSA) and *calf-thymus* DNA (CT DNA) were performed, aimed at obtaining information about the ability of compounds to inhibit the supercoiled DNA relaxation mediated by human topoisomerase IB (Top IB). Cell-based assays were also performed to study the in vitro cytotoxicity of the compounds against tumor and nontumor cell lines to gain information on the possible induction of apoptotic cell death on cell cycle effects.

RESULTS AND DISCUSSION

Synthesis and Characterization of the Ruthenium Complexes. The ruthenium complexes were synthesized by reaction of the *cis*-[$RuCl_2$(dppb)(dphppy)] precursor with the corresponding mercapto ligand in a methanol solvent. The compounds (Figure 1) were obtained as yellow solids in good yield. The compounds were characterized by several techniques, confirming their structure and purity in the solid state and solution.

X-ray Crystal Structures. The X-ray crystal structures of the three compounds were determined, and their ORTEP diagrams are shown in Figure 2. Crystallographic data are given in Part II of the Supporting Information, and selected bond lengths and angles are listed in Table 1. All complexes show a typical distorted octahedral coordination geometry around the

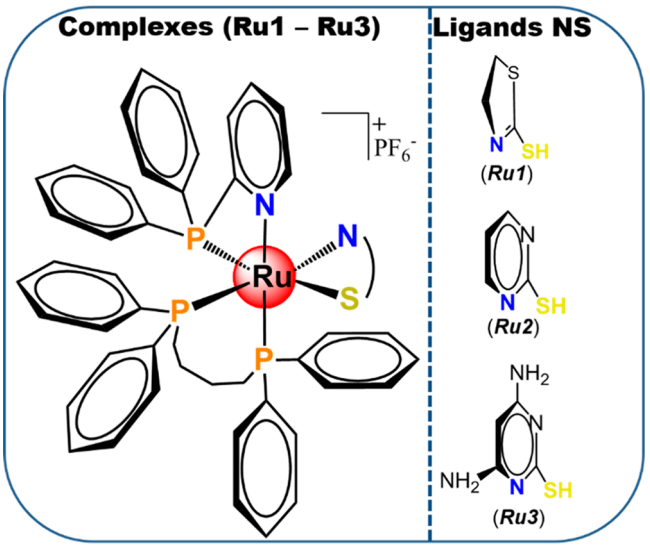

Figure 1. General chemical structures of complexes **Ru1**−**Ru3**.

ruthenium(II) center (Figure 2). In all cases, chelation of the mercapto ligand to ruthenium(II) was through the N2 atom coordinated in the equatorial plane trans to P2 and by the S1 atom, which occupies the axial position in the structure, trans to the P1 atom. The Ru−N2 and Ru−S1 bond distances are in the ranges of 2.16−2.25 and 2.39−2.43 Å, respectively, and are in the normal ranges for such ruthenium(II) compounds.[22,26,32] The mercapto ligands, coordinated to the metal, are negatively charged with electron delocalization on S2···C2···N1. The C−S bond lengths (1.71−1.73 Å) in the complexes show partial double-bond character compared to the bond lengths of the thiol (∼1.81 Å) and thione (∼1.68 Å) tautomeric forms of the free ligands, and the N1−C2 bond distances (1.34 Å) are shorter upon coordination (∼1.38 Å in the free ligand).

In the structures, the dphppy ligand is coordinated to the ruthenium metal in a P,N-chelating mode, forming a four-membered chelate ring with a bite angle in the range of 67.0−67.5°. The pyridyl ring provides limited flexibility to the ligand, where the phosphorus atom is pulled "off-axis" toward the pyridine nitrogen atom.[43] Similarly, the other angles of the chelate are strongly tensioned because of the presence of four-membered rings. Because of this ring strain, in several ruthenium complexes reported in the literature, the dphppy ligand coordination to the metal occurs monodentately, through the phosphorus atom, because it is a stronger π-acceptor atom than the nitrogen atom.[44,45]

Complexes **Ru2** and **Ru3** present intramolecular π,π-stacking interactions between the C32-phenyl ring from the P3-dppb ligand and the respective mercapto ligand. From analysis of the intramolecular stacking parameters, by the *PLATON* program, it can be observed that the centroid−centroid distance has values in the range of 3.64−3.84 Å. For compound **Ru2**, weak intermolecular interactions were observed involving the S-mercapto ligand acting as a hydrogen acceptor and the hydrogen atom from the CH2-dppb ligand acting as a donor atom. The intermolecular distance between the CH2···S forms is 2.88 Å (**Ru2**), forming dimers[46] (figure in Part II of the Supporting Information).

1D and 2D NMR Spectra. The correlation between the phosphorus atoms with their respective aromatic rings is unusual in the assignments of the NMR spectra of the

https://dx.doi.org/10.1021/acs.inorgchem.0c01835
Inorg. Chem. XXXX, XXX, XXX−XXX

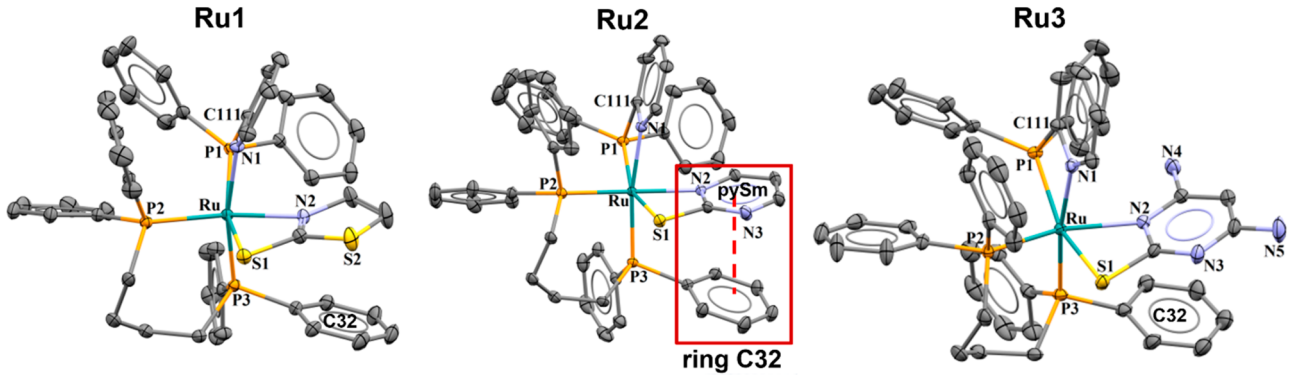

Figure 2. ORTEP views of the compounds showing the atom labels and 50% probability ellipsoids. All hydrogen atoms and anions are omitted for clarity.

Table 1. Selected Bond Lengths (Å) and Angles (deg) for Complexes

	Ru1	Ru2	Ru3
	Bond Distances (Å)		
Ru−N1	2.186(6)	2.145(2)	2.148(3)
Ru−P1	2.354(10)	2.363(7)	2.392(11)
Ru−P2	2.308(11)	2.332(7)	2.328(11)
Ru−P3	2.308(11)	2.329(7)	2.313(12)
Ru−N2	2.195(3)	2.157(2)	2.249(4)
Ru−S1	2.433(10)	2.415(7)	2.391(12)
S1−C1	1.708(4)	1.722(3)	1.731(5)
	Bond Angles (deg)		
P2−Ru−P3	95.2(4)	95.9(3)	96.2(4)
N2−Ru−S1	66.5(9)	67.3(7)	66.6(10)
N1−Ru−P3	167.5(9)	171.1(6)	171.1(10)

ruthenium diphosphine complexes. In this work, these correlations and all of the NMR signals for the compounds were assigned. The NMR data are presented in Part I of the Supporting Information. For all complexes, the $^{31}P\{^{1}H\}$ NMR spectra present AMX pattern spin systems. The two double doublets in the shielding region of the spectra refer to the nonequivalent phosphorus atom of the dppb ligand, where the P_A atom is trans to the nitrogen atom from the mercapto ligand and the P_M atom is trans to the sulfur atom from the mercapto ligand. The P_X (the phosphorus atom from the dphppy ligand) chemical shift of the synthesized complexes exhibited a shielding shift compared to the uncoordinated ligand (δ −3.88) due to the four-membered tensioned chelate ring with a P−Ru−N angle of average 67°.

The poorly resolved patterns of resonances in the ^{1}H NMR spectra are consistent with the low symmetry of the complexes. The phenyl groups from the phosphine ligands of each compound are nonequivalent, and the resonances are overlapped. The experiment of $^{1}H-^{31}P$ HMBC NMR using 12 Hz as a short-range coupling constant is particularly elucidative, allowing the unambiguous determination of coupling between the *o*-hydrogen atoms of each phenyl ring with their respective phosphorus atoms. For the dphppy ligand, an additional coupling regarding H_2 and P_X can be observed. For all complexes, the phenyl *o*-hydrogen chemical shifts follow a characteristic order of the rings: $P_{A1} > P_{X1} > P_{X2} \sim P_{A2} > P_{M1} > P_{M2}$. Furthermore, in the $^{1}H-^{31}P$ HMBC NMR, a correlation between phosphorus and hydrogen atoms can be observed using 6 Hz for long-range coupling constants. The coupling of P_M with H_a and H_b from the 2-mercaptopyrimidine ligand (Figure 3B) with four and five bindings of distances between the atoms, respectively, can be observed in **Ru2** (Figure 3). Because of the complexity of the multiplicity of the hydrogen signals, phosphorus decoupling of the hydrogen spectrum (see Part I of the Supporting Information) was performed by

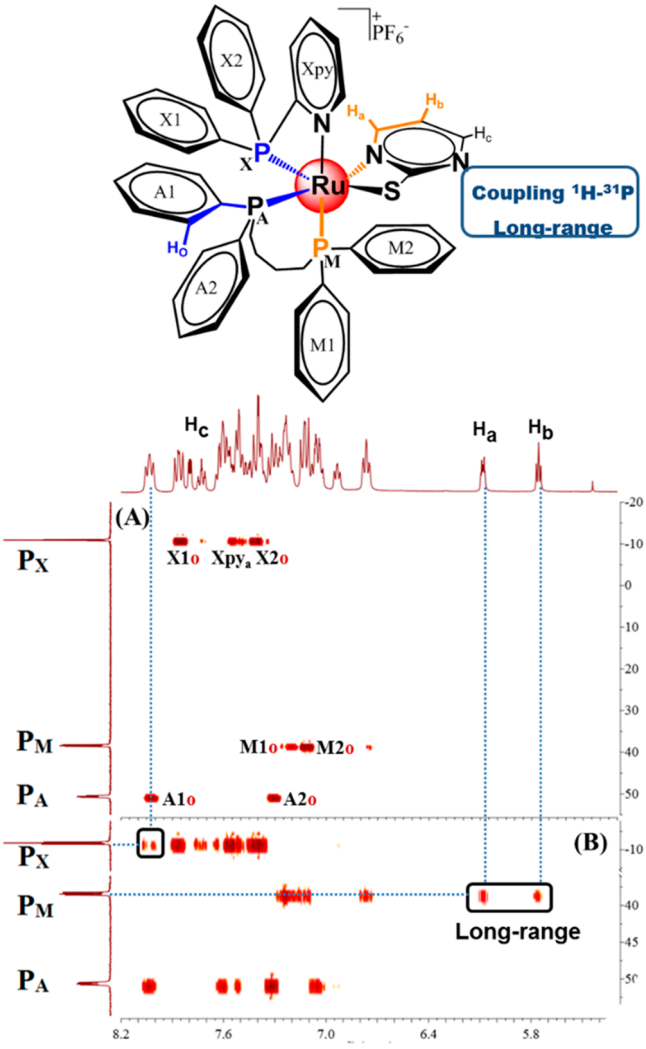

Figure 3. $^{1}H-^{31}P$ HMBC NMR contour plot for the deshielding region using 12 Hz (A) and 6 Hz (B) as long-range coupling constants of **Ru2** in CD_3CN at 298 K.

https://dx.doi.org/10.1021/acs.inorgchem.0c01835
Inorg. Chem. XXXX, XXX, XXX−XXX

Table 2. IC_{50} Values[a] (μmol L^{-1}) of the in Vitro Cytotoxic Activity against the Lung Cancer A549, Aggressive Breast Tumor MDA-MB-231, and MRC-5 (Lung) and MCF-10A (Breast) Nontumor Human Cell Lines after 48 h of Incubation with the Synthesized Complexes, Precursor Complex, Mercapto Ligands,[b] and Cisplatin (Reference Drug)

	lung cell lines			breast cell lines		
	IC_{50} (μmol L^{-1})			IC_{50} (μmol L^{-1})		
complex	A549	MRC-5	SI[c]	MDA-MB-231	MCF-10A	SI[d]
Ru1	0.23 ± 0.03	0.99 ± 0.11	4.3 ± 0.7	0.17 ± 0.01	0.30 ± 0.05	1.8 ± 0.3
Ru2	0.12 ± 0.01	0.88 ± 0.05	7.1 ± 0.7	0.14 ± 0.01	0.42 ± 0.02	3.0 ± 0.2
Ru3	1.78 ± 0.67	3.73 ± 0.15	2.1 ± 0.8	0.36 ± 0.03	0.58 ± 0.02	1.6 ± 0.1
precursor	9.76 ± 1.57	5.20 ± 0.67	0.5 ± 0.1	3.51 ± 0.56	4.07 ± 0.28	1.1 ± 0.2
cisplatin	14.42 ± 1.42	29.09 ± 0.78	2.1 ± 0.2	2.44 ± 0.20	23.9 ± 0.70	9.8 ± 0.8

[a]Data are expressed as mean ± standard deviation (n = 4). [b]For the free ligands, in all cases, IC_{50} > 50 μM. [c]SI = IC_{50}(MRC-5)/IC_{50}(A549). [d]SI = IC_{50}(MCF-10A)/IC_{50}(MDA-MB-231).

applying different decoupling irradiation values. As expected, simplification of some multiplets, such as *o*-hydrogen atoms, among others, is evident. However, a strong influence of the phosphorus nucleus was observed, especially in the signals of $H_{Xpy4''}$ of the py-dphhpy ring and $H_{A(2'')}$ of the pySm ligand (Figure S23). Partial phosphorus decoupling of the ^{1}H NMR spectra of complex **Ru2** (Part I of the Supporting Information and Figure S23) resulted in collapse of the triplet of triplets ($H_{Xpy4''}$) to a broad triplet, while the pseudo double triplet (dt) of pySm collapsed to a double doublet (dd). The resonances of the mercapto ligands are shielding shifts compared to the free ligand resonances. As can be seen, in the solid state, in the X-ray structures of the complexes, these hydrogen atoms are influenced by the magnetic anisotropy shielding cone of the C32-phenyl ring of the P3-dppb ligand, which justifies the greater deshielding compared to the other hydrogen atoms of the compounds.

Electrochemical Studies. The electrochemical behavior of the complexes was studied by cyclic voltammetry using a platinum-disk working electrode in a dichloromethane solvent containing a 0.1 M tetrabutylammonium hexafluorophosphate electrolyte. In scans toward the positive potential, all complexes exhibit one oxidation process associated with quasi-reversible Ru(II)/Ru(III) conversion. The redox couple corresponded to a quasi-reversible process, with half-wave potential ($E_{1/2}$) values in the range of 1.1−1.4 V versus Ag/AgCl (Part III of the Supporting Information). This character of the ruthenium-centered processes is in agreement with those previously reported for similar Ru(II)-phosphine complexes with mercapto ligands.[21,25] The half-wave potential [Ru(II)/Ru(III)] values ($E_{1/2}$) are modulated by the contribution of the donor/acceptor properties of the ligands present in the coordination sphere of the metal center in the complexes. The character π receptor of the phosphine ligands (dppb and dphppy) and also of the mercapto ligands stabilizes the lower oxidation state of Ru(II). Thus, the complexes synthesized here show a higher Ru(II)/Ru(III) potential compared with the analogue complexes, $[Ru(NS)(dppb)(bipy)]PF_6$,[25] as expected for the better π-receptor properties of the ambidentate dphppy ligand (P−N ligand) compared to the bipyridine molecule (N−N ligand). Moreover, replacement of the chlorido ligands (good σ/π-donating ability) by the mercapto ligand (poor σ-donor and moderate π-acceptor properties) induces to a decrease in the electron density on the Ru(II) center.

Chemical Behavior of Compounds in an Aqueous Medium. Before studies on the cytotoxicity and interaction of the complexes with biomolecules, their stabilities in dimethyl sulfoxide (DMSO), cell culture media, and buffered aqueous media were investigated by $^{31}P\{^1H\}$ NMR spectroscopy over a time of 48 h. The complexes are not soluble in a pure aqueous medium; however, they are soluble in a mixture of 1:99 DMSO/aqueous media at micromolar concentrations. For all complexes, there were no changes in their $^{31}P\{^1H\}$ NMR spectra, demonstrating their integrity in aqueous media and DMSO throughout the experiments.

In Vitro Cytotoxicity. The cytotoxic activity of the complexes was assessed against the lung cancer A549 cell line, the aggressive breast tumor MDA-MB-231 cell lines, and the MRC-5 (lung) and MCF-10A (breast) nontumorigenic human cell lines. In general, the complexes were found to be active for all studied tumor cell lines, with low IC_{50} values (Table 2), remarkably surpassing the cisplatin activity in these cell lines. The ruthenium complexes were also more cytotoxic than the complex precursor, showing a satisfactory effect upon coordination of the mercapto ligand to ruthenium, as well as the respective free phosphines and uncoordinated mercapto ligands. These results demonstrated possible synergisms between the metallic center and functional ligands.

In general, the cytotoxic activity of the compounds follow a characteristic order for both tumor cell lines, **Ru3** < **Ru1** < **Ru2**. For complexes **Ru1** and **Ru2**, there are no significant differences between their IC_{50} values, and structurally they are characterized by "simple rings" of the mercapto ligands. However, complex **Ru3** presented lower cytotoxicity in the series of compounds and is characterized by presenting functional groups attached to the rings from the mercapto ligands, such as donor groups, to the amine. In particular for the lung cancer A549 cell line, this behavior is observed. **Ru2** displayed an IC_{50} value that was 2 times lower than that of complex **Ru1**, and mainly compounds **Ru2** and **Ru1** were 15 and 8 times, respectively, more cytotoxic in relation to **Ru3**. Furthermore, as can be seen in Table 2, complex **Ru3** is the least selective for both cancer cells.

Lipophilicity is an important property that may be related to the ability of a compound to permeate through biological membranes by passive diffusion. All complexes showed better affinity by the organic phase, with values of the distribution coefficient (log P) of 1.34 ± 0.28, 1.14 ± 0.22, and 0.88 ± 0.31 for **Ru1**−**Ru3**, respectively. The complex with the amine groups presents less lipophilic character. Certainly, the phosphine ligands, dppb and dphppy, contribute to the lipophilic nature of the compounds. There was a good correlation between the hydrophobicity and cytotoxicity of

https://dx.doi.org/10.1021/acs.inorgchem.0c01835
Inorg. Chem. XXXX, XXX, XXX−XXX

the complexes, where the less hydrophobic complex shows worse cytotoxic activity, while complexes **Ru1** and **Ru2**, which have practically the same lipophilicity, have similar cytotoxicities.

For the MDA-MDB-231 cells, the cytotoxicity between complexes is less discrepant, in which the IC_{50} values for complexes **Ru1** and **Ru2** do not show a significant difference. However, complex **Ru3** is slightly less cytotoxic, exhibiting an IC_{50} of approximately 2 times lower compared to those of the other complexes. Again, the results are in accordance with the lower lipophilic character of the compound.

The IC_{50} values for the complexes are equal or lower compared to those of similar complexes previously reported by our group, $[Ru(NS)(bipy)(dppb)]PF_6$[25] and $[Ru(NS)(bipy)(dppf)]PF_6$.[23] For example, in the A549 cells, **Ru3** (IC_{50} = 2.59 ± 0.19 μM; IS = 6.7) displayed an IC_{50} value that is 4 times lower compared to that of the analogue complex with bipy, $[Ru(damp)(bipy)(dppb)]PF_6$ (IC_{50} = 11.74 ± 0.52 μM; IS = 1.0).[25] Complex **Ru1** (IC_{50} = 0.23 ± 0.03 μM; IS = 4) displayed an IC_{50} value for the A549 cancer cells that is statistically equal compared to that of the analogue complex with bipy, $[Ru(tzdt)(bipy)(dppb)]PF_6$ (IC_{50} = 0.21 ± 0.05 μM; IS = 17).[25] However, the complex with the bipy ligand showed better selectivity. In comparison to the classes of ruthenium(II) polypyridyl[47−51] and iridium/ruthenium arene[52−59] complexes, the ruthenium(II) diphosphine compounds containing mercapto ligands (NS) are more cytotoxic in several cancer cell lines.

It is worth mentioning that an important factor to take into consideration is the selectivity for cancer cells. The complexes were more active for the A549 and MDA-MB-231 tumor cell lines compared to the corresponding nontumor cell lines MCF-10A and MRC-5, respectively. It is also worth mentioning the better selectivity indexes (SIs) in the cell-line pair MRC-5/A549 compared to the SI of cisplatin. Complex **Ru2** was more selective than the other two compounds and also 3 times more selective than cisplatin. Because of the better selectivity of complex **Ru2** for A549 lung cancer cells with a value of 7.1, it was chosen for further evaluations as an inducer of cell death in A549 lung cancer cells.

Morphological Observations in Cells. Morphological changes in the A549 cells (Figure 4A) treated with complex **Ru2** in different concentrations, over 48 h, were evaluated using an inverted microscope. The treatment of A549 cells with complex **Ru2**, at concentrations of IC_{50} and 2 × IC_{50} after 24 h, promotes the appearance of elongated cells compared to untreated control cells. In 48 h of treatment at concentrations of IC_{50} and $^1/_2$ × IC_{50}, the density of cells decreased and most of them presented elongated features. At a concentration of 2 × IC_{50} in 48 h, most cells presented round features and were nonadherent in culture. These morphological changes indicate that compound **Ru2** is capable of inducing cell death by apoptosis in A549 cells.[14] There are also no signs of cell death via necrosis, such as a loss of cell membrane integrity.

Inhibition of Cell Migration. The effects of complex **Ru2** on cell migration were evaluated by wound-healing assay (Figure 4B). This assay consists of removing cells from an area, in this case mechanically, creating a wound (i.e., a cell-free zone) in a confluent monolayer, and evaluates the closure of the wound.[60] The complex concentrations used do not cause cell death, which ensures that the changes in the wound area are predominantly due to cell migration. Upon treatment of A549 cells with complex **Ru2** at concentrations of $^1/_4$ × IC_{50} and $^1/_2$ × IC_{50} for 48 h, the wound closure was inhibited in approximately 5% and 18%, respectively, compared to those of untreated cells.

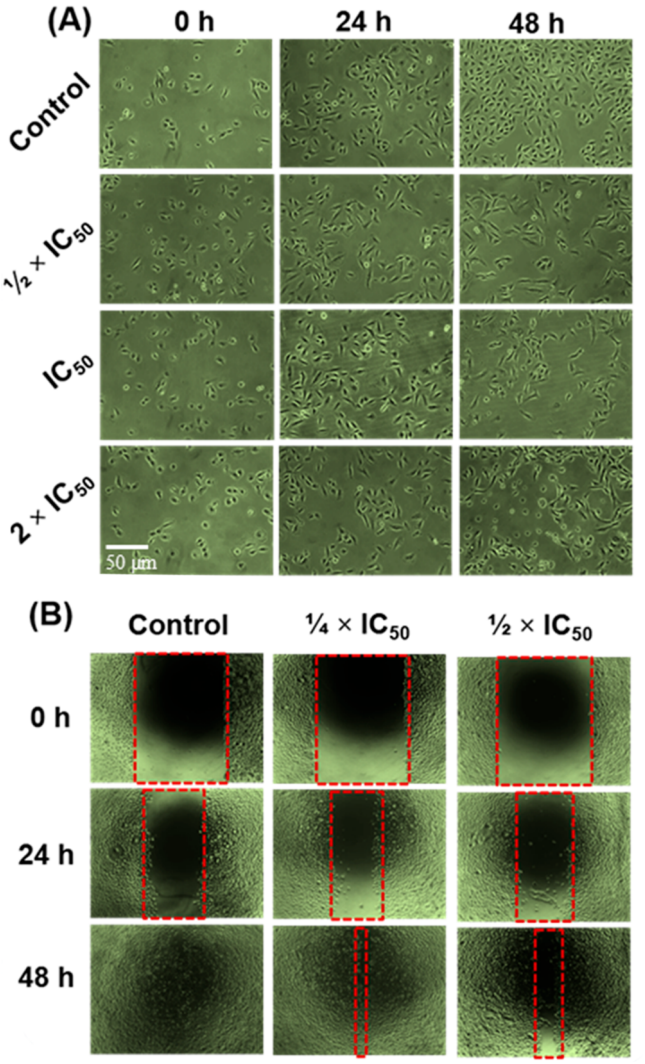

Figure 4. (A) Microscopy images of A549 tumor cells showing the cellular morphology after treatment with different concentrations of complex **Ru2**. (B) Microscopy images monitoring the migratory capacity of the untreated A549 tumor cells (control) and cells treated with different concentrations of complex **Ru2** by wound-healing assay.

Apoptosis Assay. 7-Aminoactinomycin D (7-AAD)/annexin V-PE cytometry-based assay is used to evaluate the process of programmed cell death in response to a cytotoxic agent. A549 tumor cells were treated with complex **Ru2** at 0.5, 1.0, and 2.0 equipotent concentrations of IC_{50} for 48 h and analyzed by flow cytometry in conjunction with the dyes to determine apoptotic and necrotic cell populations. As shown in Figure 5A, complex **Ru2** at a concentration of 0.5 × IC_{50} led to 17.5% of A549 cells in early apoptotic phases after 48 h. When the concentration of the complex was increased, the annexin V-PE positive cell population also increased compared to that of the untreated control. At a concentration of 2 × IC_{50} of complex **Ru2**, the total proportion of early apoptotic cells was 40.3%, whereas untreated cells remained 93% viable. At all concentrations, the complex induced early apoptotic cell death in a concentration-dependent manner and no cell death from necrosis was observed.

https://dx.doi.org/10.1021/acs.inorgchem.0c01835
Inorg. Chem. XXXX, XXX, XXX−XXX

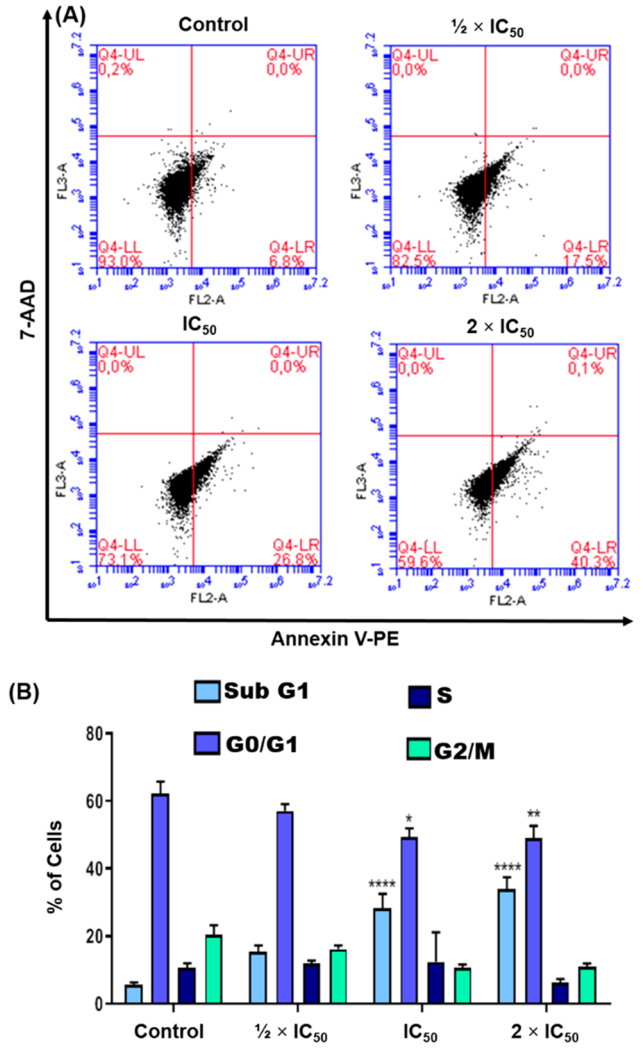

Figure 5. (A) Apoptosis analysis of A549 cells after 48 h of exposure to complex **Ru2** determined by flow cytometry using annexin V-PE versus 7-AAD staining. The concentrations used were 0.5, 1.0, and 2 equipotent to IC50. (B) Histogram cell cycle distribution of A549 cells after 48 h of exposure to complex **Ru2**. The concentrations used were 0.5, 1.0, and 2 equipotent to IC_{50}. Cell staining for flow cytometry was carried out using PI/RNase. The error bars represent the standard deviations from three independent experiments. The results are mean ± standard deviation (n = 3). (****) $p < 0.0001$ compared with the value of the control.

Cycle Cell Analysis of the A549 Cells. The ability of compound **Ru2** to disrupt the cell cycle progression in a manner that reflects that its mechanism of action was investigated. A549 tumor cells were synchronized at the G1/S phase using serum starvation, and the cell cycle progression of untreated and compound-treated cells was evaluated by flow cytometry using propidium iodide (PI) labeling (Figure 5B). Treatment of the A549 cells with complex **Ru2** at different equipotent concentrations of IC_{50} ($^1/_2 \times IC_{50}$, 1.0 × IC_{50}, and 2.0 × IC_{50}) for 48 h led to an increase in the population of cells at the Sub-G1 phase in a concentration-dependent manner compared to untreated cells. The percentages of cells at the Sub-G1 phase increased from 5.5% (untreated cells) to 15.5% ($^1/_2 \times IC_{50}$), 28.3% (IC_{50}), and 33.9% (2 × IC_{50}) after treatment, which is related to a decreased DNA content due to fragmentation. Consequently, the percentages of cells arrested at the G0/G1 phase were slightly decreased after **Ru2** was added compared to the control cells. Additionally, the increase in cells at the Sub-G1 phase confirms the efficiency of the complex regarding the induction of cellular apoptosis and acts in a manner dependent on the cell cycle status because regulated forms of cell death, such as apoptosis, generally depend on specific checkpoints within the cell cycle to mediate these processes.[61,62]

Cellular Uptake. The cellular uptake characteristic of complexes is an important factor to be correlated with their cytotoxic effects and bioactivities. For complex **Ru2**, the most lipophilic of the complex series, accumulation of the ruthenium metal from **Ru2** was quantitatively determined in the A549 tumor adherent cells and in the culture medium by inductively coupled plasma mass spectrometry (ICP-MS; Figure 6). The

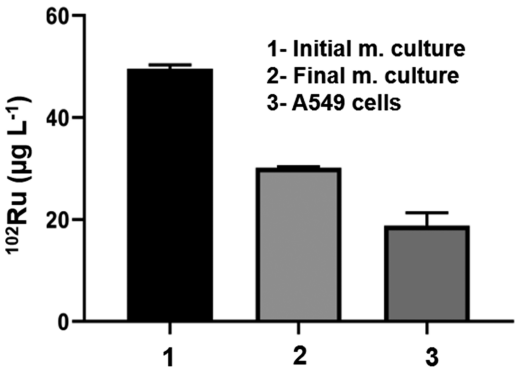

Figure 6. Complex concentration ($\mu g\ L^{-1}$) in a medium culture and in A549 cells exposed to compound **Ru2**. The metal content was determined by ICP-MS after an incubation time of 24 h at 0.5 μM compounds. Data are expressed as mean ± SEM of three independent assays.

cellular ruthenium concentration was determined after 24 h of exposure to 0.5 μM **Ru2**, and the results were reported as micrograms of ruthenium per liter. In this period, the uptake level in A549 cells treated with **Ru2** represents around 38% of the initial amount of ruthenium (18.8 ± 2.5 $\mu g\ L^{-1}$), while in the final culture medium, it was (30.2 ± 0.2 $\mu g\ L^{-1}$). The efficient accumulation of ruthenium in A549 cells is consistent with the lipophilicity of the complex, which certainly facilitates the influx of the ruthenium(II) complex through the cell membrane by passive diffusion.

HSA Binding Study by Fluorescence Quenching. HSA stands out as the most important nonspecific transporter protein in the circulatory system. Serum albumin can play a crucial role in drug biodistribution, transport, release, and toxicity. Albumin binding is of great importance in terms of understanding drug pharmacokinetics and drug−protein interactions.[63,64]

For complexes **Ru1**−**Ru3**, the HSA fluorescence intensity gradually decreases with increasing concentration of the complexes, suggesting that the microenvironment of the Trp-214 residue of HSA was altered when the metal complexes were added, as shown by the fluorescence spectra of HSA (Figure 7A) in the presence of an increasing amount of complex **Ru1** (for other compounds, see Part IV of the Supporting Information). Static quenching, which usually causes perturbation of the absorption spectrum of the fluorophore, is operative in this system.[65] This can be confirmed by a decrease in the Stern−Volmer constants with

https://dx.doi.org/10.1021/acs.inorgchem.0c01835
Inorg. Chem. XXXX, XXX, XXX−XXX

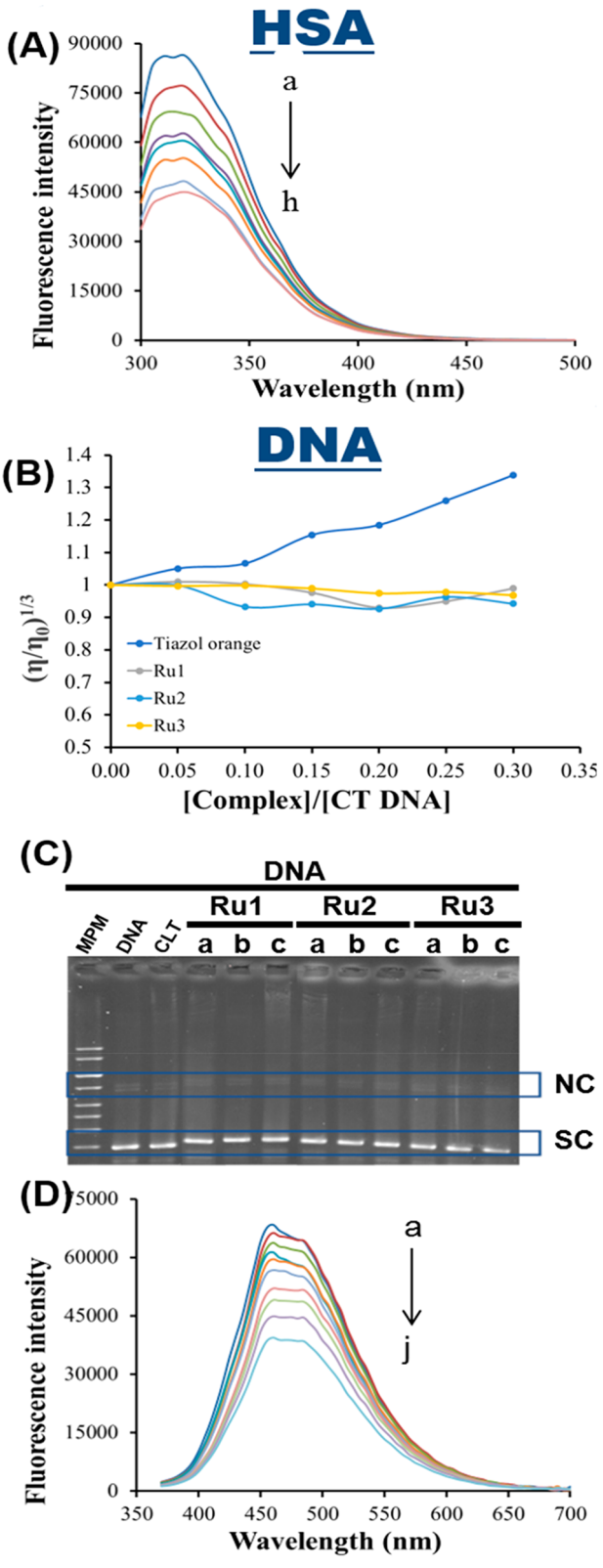

Figure 7. (A) Fluorescence quenching spectra of HSA (5 μM) in the absence and presence of compound **Ru1** at different [compound]/[HSA] ratios (a, 0; b, 1; c, 2; d, 3; e, 4; f, 5; g, 6; h, 7) with an excitation wavelength at 270 nm at 310 K in a Tris-HCl buffer. The arrow indicates an increase of the quencher concentration. (B) Effect of the increasing concentration of complexes on the relative viscosity of CT DNA. [DNA] = 200 μM. (C) Electrophoresis mobility shift assays of plasmid pBR322 in the absence and presence of the compounds. DNA/buffer refers to untreated plasmid in a Tris-HCl buffer. Parts a–c correspond to the [compound]/[plasmid] ratios of 0.25, 0.50, and 1.0, respectively. (D) Fluorescence quenching spectra of DNA_Hoechst in the absence and presence of compound **Ru1** at different ratios with an excitation wavelength at 343 nm at 310 K in a Tris-HCl buffer. The arrow indicates an increase in the quencher concentration.

an increase in the temperature of the experiments. Besides this, the maximum value of the bimolecular quenching constant (k_q) parameter for a mechanism to be considered pure dynamic quenching is 1×10^{10} M^{-1} s^{-1}.[66] For all complexes, the bimolecular quenching constant (k_q) values obtained were higher than 1×10^{10} M^{-1} s^{-1}, supporting that the mechanism is static.

The magnitudes of the binding constant values are 10^5–10^7, indicating the formation of a moderate-to-strong interaction between complexes and the protein (Part IV of the Supporting Information). The number of binding sites for HSA/complex interaction indicates one binding site HSA by the ruthenium complex. The thermodynamic parameters were analyzed to evaluate the main intermolecular forces involved in the interactions between the compounds and HSA. For all complexes, the positive ΔH and ΔS values, according to Ross and Subramanian,[65] indicate that the insertion of compounds in the protein framework occurs through hydrophobic interactions. The negative values of ΔG reveal that the interaction processes between the compounds and HSA are spontaneous.[65,67]

Interaction with DNA. DNA is one of the most important and studied biological targets for coordination compounds with anticancer activity.[8] Several ruthenium complexes have their mechanisms of cytotoxic action against tumor cells associated with direct interactions with DNA.[67] Therefore, the binding modes of the complexes with DNA were studied by different methods (Figure 7B,C).

Viscosity. The covalent and intercalation binding modes, as well as electrostatic attraction and groove associates (weak reversible interactions) of the compounds to DNA, reflect distinct behaviors in the DNA viscosity.[68] As shown Figure 7B, the relative viscosity of CT DNA undergoes no alteration after continuous addition of the complexes, demonstrating that its interactions do not cause changes in the DNA tertiary structures. In contrast, the relative viscosity of CT DNA treated with thiazole orange increased significantly upon the addition of the classic intercalating ligand due to prolonged double strands of DNA. These results suggest that the complexes exhibit a weak binding ability with CT DNA.[69] The intercalative and covalent binding modes are discarded by the viscosity results.

Electrophoretic Mobility of the Plasmid DNA in Gel Agarose. Figure 7C shows the electrophoretic mobility of the plasmid pBR322 in the presence of increasing amounts of complexes in gel agarose. Lane 3 (CTL) represents the pattern of migration of the plasmid DNA with DMSO, which is observed in forms I and II. Form I is the DNA that assumed the supercoiled conformation (SC), and form II is the open circular conformation (CC), which is more relaxed compared to supercoiled DNA and presents less electrophoretic mobility. The pattern of the electrophoretic mobility of the plasmid sample treated with different concentrations of the complexes

https://dx.doi.org/10.1021/acs.inorgchem.0c01835
Inorg. Chem. XXXX, XXX, XXX–XXX

is the same migration pattern as that of the untreated DNA. It thus appears that **Ru1**−**Ru3** are not capable of inducing noticeable alterations in the tertiary structure of the plasmid that are reflected in the electrophoretic mobility.

Displacement Assay with Hoechst 33258. The interactions of the complexes with CT DNA were also assessed by fluorescence−dye displacement studies using the Hoechst 33258 dye. The Hoechst has an emission at 490 nm of low fluorescence quantum yield. However, the binding of Hoechst 33258 in the minor groove of B-DNA provides an intense fluorescence quantum yield for the Hoechst/DNA system.[17,70] The results of the Hoechst/DNA complex achieved in the presence of equivalent amounts of the compounds in relation to Hoechst. Figure 7D shows significant fluorescence quenching of the Hoechst/DNA complex in the presence of **Ru2**. A decrease in the CT DNA fluorescence intensity was observed with increasing amounts of the complexes in the solution for all complexes. In the higher molar ratio ($r = 1$), the fluorescence intensity of CT DNA/Hoechst was approximately 49−42% of the initial value. The quenching fluorescence indicates that interaction of the compounds causes minor changes in the region around of the DNA minor groove, leading to partial ejection of the Hoechst of the DNA minor groove.

General Aspects of Interaction of the Complexes with DNA. Studies of the viscosity (Figure 7B) and electrophoretic mobility (Figure 7C) of the plasmid DNA in gel agarose suggest that the compounds do not lead to conformational altercation in the tertiary and secondary DNA structures. Not surprisingly, interaction studies clearly show that some binding modes can be discarded, including irreversible DNA covalent binding and intercalation, which is consistent with structural features of the complexes. In the Trisma-HCl buffer (10% DMSO), the **Ru1**−**Ru3** complexes are stable. Thus, by analysis of the data obtained from the studied techniques, mainly the displacement assay of Hoechst 33258 (Figure 7D), it can be suggested that the DNA binding modes of the complexes with DNA are weak and reversible interactions, which occur by the minor groove. Interactions through DNA grooves are based on a set of intermolecular interactions,[71] such as hydrophobic, electrostatic, van der Waals, and hydrogen bonding, and are consistent with the structural characteristics of the complexes. Upon analysis of the results, it can be suggested that the "trigger" for cell death does not involve "direct action" of the complexes with DNA. The "trigger" must be associated with other biological targets, especially targets overexpressed in tumor cells that justify the good selectivity of the compounds.

Top IB Inhibition Assay in Plasmid DNA Relaxation by Ruthenium Compounds. DNA topoisomerases are nuclear enzymes that control and modify the topological state of DNA. These enzymes are involved in many vital cellular processes, such as DNA replication, chromosome condensation, and chromosome segregation.[72] Specifically, the enzyme type Top IB catalyzes the formation of single-strand breaks in DNA, in a catalytic cycle of five main steps.[73,74] In tumor cells, a high level of Top IB enzyme is maintained, and thus it has been considered to be a target for antitumor agents.[75−77] To highlight the multitargeted character of the compounds, their capacity to inhibit the Top IB catalytic process was investigated by relaxation assay of the supercoiled plasmid. Initially, it was found that complexes do not alter the pattern of migration of the DNA supercoiled plasmid.

In Figure 8, lane 1 represents the negative control (pattern of migration of the DNA plasmid), where only the band of the

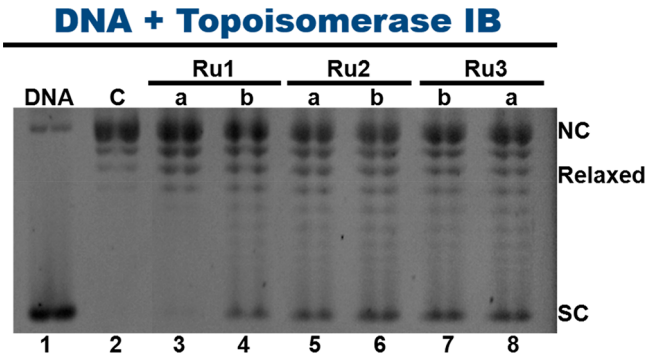

Figure 8. Electrophoresis mobility shift assay of the plasmid pBR322 relaxed by a human Top IB catalytic process by agarose gel electrophoresis in 1% agarose gel in the presence of the following concentrations of the complexes (lanes 3−8); a, 0.5 μM; b, 5 μM.

supercoiled form (SC) can be observed. Lane 2 represents the pattern of the electrophoretic mobility of the DNA plasmid after the process of relaxation catalyzed by human topoisomerase. The action of the enzyme produces several circular forms (NC) with slower electrophoretic mobility compared to that of supercoiled DNA. At the concentration 0.5 μM, complexes **Ru2** and **Ru3** (as shown in lanes 5−8) partially inhibited the activity of Top IB. Complex **Ru1** (as shown in lanes 3 and 4) showed an inhibition of partial Top IB activity at the concentration 5 μM. It should be noted that the complexes are capable of inhibiting the Top IB catalytic activity, even partially, at low concentrations. In these concentrations, the complexes have high cytotoxic activity against cancer cell lines. Although the mechanism of action of the complexes cannot be proposed, it can be seen that the Top IB enzyme is one of the efficient targets for the class of compounds studied here ruthenium(II) diphosphine with mercapto ligands.

Effect of Ruthenium Compounds on the Proteasome Activity in Cells. To investigate the inhibitory effects of the ruthenium compounds through direct interaction with the proteasome (Figure 9E), assays with purified 20S proteasome were performed. At low concentrations, complexes **Ru2** and **Ru3** inhibited the chymotrypsin-like activity of the 20S proteasome in 69% and 90%, respectively. On the other hand, complex **Ru1** had no proteasome inhibitory effect because the enzymatic activity remained the same as that of the controls. The reversible proteasome inhibitor MG132, used as a positive control, caused inhibition in 99%.

To evaluate the effects of compounds on the proteasome activity in intact cells, HEK293T cells were treated with each compound for different times. HEK293T cells stably express a short-lived green fluorescent protein (GFP), which is accumulated under proteasome inhibition.[78] For assay, the complex concentrations used do not cause the induction of cell death. After the cells were treated with the MG132 inhibitor, an increasing accumulation of GFP was observed, which indicates that the model used was functioning properly (Figure 9A). After 2 and 4 h of treatment of the cells, there was minimal variation in the percentage of GFP accumulated in the cells compared to the control cells. The greatest variation occurred after 24 h of treatment, and the cells treated with complex **Ru3** (Figure 9D) significantly inhibited the

https://dx.doi.org/10.1021/acs.inorgchem.0c01835
Inorg. Chem. XXXX, XXX, XXX−XXX

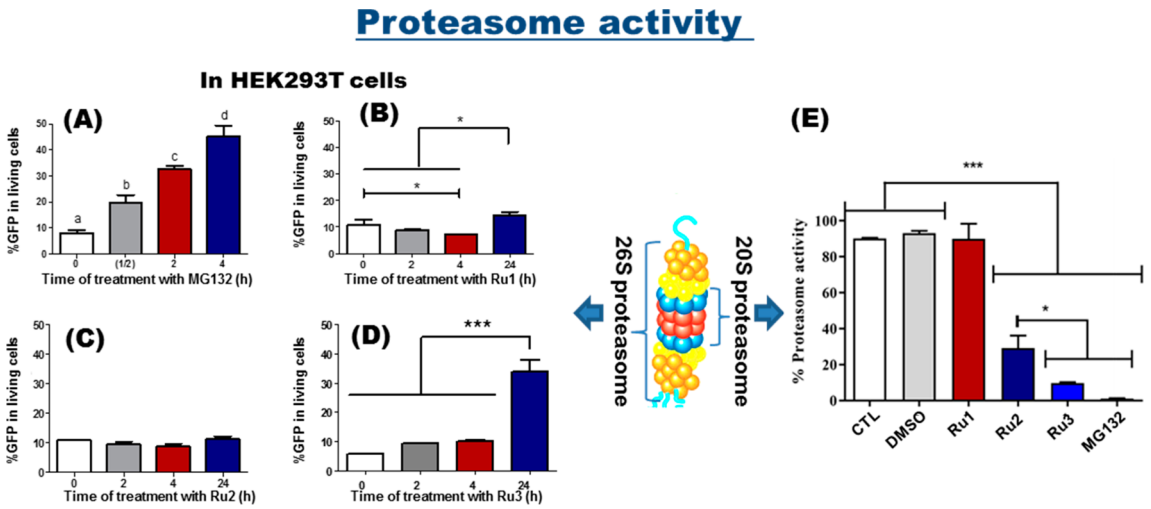

Figure 9. In vitro proteasome inhibition by complexes **Ru1** (1 μM), **Ru2** (0.9 μM), and **Ru3** (3.7 μM). HEK293T-uGFP cells were treated with the proteasomal inhibitor MG132 (10 μM) as the positive control (A) or the ruthenium complexes **Ru1** (B), **Ru2** (C), and **Ru3** (D) at the indicated period and concentration. The *Y* axis represents the percentage of cells expressing GFP related to viable cells. (E) Purified 20S proteasome was used to quantify the capacity of ruthenium complexes to directly inhibit proteasome. MG132 was also used as the positive control. The *Y* axis represents the percentage of 20S proteasome activity under each treatment. Assays were performed in experimental triplicate, and data dispersion is shown in the error bar. The ANOVA one-way test was applied with *Prism 5* (GraphPad, USA).

proteasome chymotrypsin-like activity. Interestingly, after 24 h of treatment with **Ru1** (Figure 9B), the percentage of GFP of the cells (14.2 ± 1.5%) was not statistically different from that at 0 h (10.7 ± 2.2%), indicating that the compound had no ability to inhibit the proteasome in cells. Surprisingly, **Ru2** (Figure 9C) had no proteasome inhibitory effect in HEK293T cells. In this case, we suggest that, possibly in the intracellular environment, complex **Ru2** presents interactions directed toward other biomolecules. When these preliminary assays are examined, it is clear that slight structural changes in the complexes provide distinct potencies in the proteasome inhibitory effect in cultured cell conditions. Finally, **Ru3** acts as a proteasome inhibitor in cells, which can lead to the accumulation of proteins involved in the division and death of cancer cells.

The **Ru3** complex stands out by diminishing the proteasomal activity to an extent approximately equal to the classic inhibitor MG132, at 2.5 times lower concentration. In structural terms, the hypothesis for the strong inhibitory effect by **Ru3** is due to the ability to perform hydrogen bonds by means of amine moieties of the damp ligand with the residual active groups of the enzyme, such as threonine1 (Thr1) residues of the 20S proteasome. As a reference,[79] docking studies carried out for the interaction of the enzyme with α-ketoamide (proteasome inhibitors) showed the role of hydrogen interactions. The medium/strong hydrogen bonds between inhibitors and the binding sites of the active Thr1 residues of the β1 and β2 catalytic subunits (20S proteasome) are important factors in the contacts with key residues of the binding pockets.

CONCLUSIONS

A series of new ruthenium(II) phosphine complexes with mercapto ligands were synthesized and fully characterized. The ^{1}H NMR data of the complexes are consistent with compounds of low symmetry in solution with magnetic nonequivalent *o*-hydrogen atoms of the phenyl rings. In addition, long-range phosphorus and mercapto hydrogen couplings are observed by ^{31}P{^{1}H}−^{1}H HMBC NMR. In the solid state, $\pi-\pi$ intermolecular interactions between the dppb phenyl groups and mercapto ligands provide the influence of the magnetic anisotropy shielding of some mercapto hydrogen atoms. All complexes show good cytotoxic activity against the lung cancer A549 cell line and against the aggressive breast tumor MDA-MB-231 cell line. Additionally, the complexes are more cytotoxic against the cancer cell lines than against the MRC-5 (lung) and MCF-10 (breast) nontumor human cell lines. In particular, complex **Ru2** stands out because it is about 3 times more selective in the MRC-5/A549 pair cell lines compared to cisplatin. Complexes **Ru1** and **Ru2**, which are characterized by "simple rings" of the NS ligands and greater lipophilicity, are more cytotoxic than compound **Ru3**, characterized by the presence of functional groups (amine donor groups) attached to the rings at the mercapto ligands. The A549 cells treated with complex **Ru2** showed morphological changes, compared to those of control cells, with round features and nonadherent in culture. These changes are indications of cell death by apoptosis, as confirmed by 7-AAD/annexin V-PE cytometry-based assay. The results demonstrate that **Ru2** induced early apoptotic cell death and did not induce necrosis cell death. Complex **Ru2** also showed a low capacity to inhibit cell migration, suggesting that there was no antimetastatic activity. Additionally, the complex acts in a manner dependent on the cell cycle status with an increase of the cells arrested at the Sub-G1 phase, which can trigger cellular apoptosis. Studies by ICP-MS in A549 cells showed an efficient accumulation of ruthenium in the cells after treatment with compound **Ru2**.

The complexes caused no significant changes in the tertiary and secondary DNA structures, indicating that this biomolecule is probably not their primary target. Studies with enzymatic targets, especially targets overexpressed in tumor cells that justify the cytotoxic activity of the compounds, were carried out. It was found that the complexes are capable of partially inhibiting the Top IB catalytic activity, at low concentrations, close to the IC_{50} values of cancer cell lines. In living cells, complex **Ru3** was able to inhibit the proteasomal

https://dx.doi.org/10.1021/acs.inorgchem.0c01835
Inorg. Chem. XXXX, XXX, XXX−XXX

activity. In addition, complex **Ru3** was able to diminish the proteasomal activity to an extent approximately equal to that of the classic inhibitor MG132, at a lower concentration. A hypothesis for the strong inhibitory effect of the enzyme by the ruthenium complex **Ru3** is due to its ability to perform hydrogen-bonding interactions with the residual Thr1 active groups of the enzyme, showing the importance of the amine moieties of the damp ligand. Overall, the proteasome enzyme can be a biological target for this complex. However, we suggest that **Ru2** and **Ru1** can act specifically toward other biomolecules and in the cellular environment.

EXPERIMENTAL SECTION

Materials for Synthesis. $RuCl_3 \cdot 3H_2O$, triphenylphosphine (PPh_3), 1,4-bis(diphenylphosphino)butane (dppb), diphenyl-2-pyridylphosphine (dphppy), 2-thiazoline-2-thiol (tzdt), 2-mercaptopyrimidine (pySm), and 4,6-diamino-2-mercaptopyrimidine (damp) were obtained from Sigma-Aldrich and used without further purification. All other chemicals were used as purchased.

Instrumentation. Elemental analyses were carried out using a FISIONS Instrument EA 1108 CHNS elemental analyzer at the Microanalytical Laboratory at the Federal University of São Carlos, São Carlos, Brazil. Conductivity measurements in DMSO solutions (1.0 mM) of the complexes were performed on a Meter Lab CDM2300 conductivity meter. Fourier transform infrared spectra were recorded on a Bomem-Michelson 102 spectrometer in the range of 4000−200 cm^{-1} in KBr cells. UV/visible absorption spectra were performed on a Varian Cary 500 model near-IR spectrophotometer in the range of 190−800 nm. Electrochemical measurements were carried out using a Princeton Applied Research 273A potentiostat galvanostat in a dichloromethane solution containing 0.1 M tetrabutylammonium perchlorate (TBAP; Fluka Purum). A conventional three-electrode system was used with the working and auxiliary electrodes and Ag/AgCl, 0.10 M TBAP in dichloromethane, as the reference electrode. Under these conditions, ferrocene/ferrocenium oxidation occurs at 0.43 V.

X-ray Structure Determination. All complexes were crystallized from slow evaporation of the dichloromethane/methanol solution. Single-crystal X-ray diffraction measurements were performed on an Enraf-Nonius Kappa-CCD diffractometer with graphite-monochromated Mo Kα radiation (λ= 0.71073 Å) at room temperature (293 K). Cell refinements were determined using the *COLLECT* program.[80,81] Integration and scaling of the reflections were carried out with the HKL Denzo-Scalepack software package.[82] The structures were solved through direct methods of phase retrieval with *SHELXS-2013*[83] and the refinement by full-matrix least-squares on F^2 with *SHELXL-2013S*[83] within the *WinGX-v.2013.3* program package. Absorption correction was performed by the *Gaussian* method.[84] Non-hydrogen atoms were refined anisotropically, and hydrogen atoms were fixed at calculated positions and refined using the riding mode. Structure analysis and the preparation of the artwork were performed using *MERCURY* and *ORTEP-3* software.[84] Material for publication (CIF file) was generated by *WinGX*. The crystallographic data and main refinement parameters for all complexes are summarized in Part II of the Supporting Information.

Syntheses. Syntheses of the complexes were carried out under an argon atmosphere using a standard Schlenk technique. Analytical-grade solvents were distilled from the appropriate drying agents prior to use. The precursors $[RuCl_2(PPh_3)_3]$,[85] $[RuCl_2(dppb)(PPh_3)]$,[86] and *cis*-$[RuCl_2(dppb)(dphppy)]$[87] were synthesized as described in the literature.

A general description of the synthesis of $[Ru(NS)(dppb)(dphppy)]PF_6$ compounds. The specific mercapto ligand (0.12 mmol) was added to a suspension of the *cis*-$[RuCl_2(dppb)(dphppy)]$ complex (0.12 mmol) in methanol (20 mL). The resulting solution was stirred for 12 h at room temperature. After KPF_6 (0.12 mmol) and 0.5 h of stirring, the solvent was removed, under reduced pressure, to ca. 2 mL, and diethyl ether was added for precipitation of a yellow solid. The solid was filtered off, rinsed with water (3 × 10 mL) and diethyl ether (5 × 10 mL), and dried in vacuo.

The solids were characterized by NMR spectra ($^{31}P\{^1H\}$, ^1H, and $^{13}C\{^1H\}$), and all signals were unequivocally assigned and are summarized in Part I of the Supporting Information.

$[Ru(tzdt)(dppb)(dphppy)]PF_6$ (Ru1). Compound **Ru1** was synthesized following the general procedure of the synthesis using 100 mg (0.12 mmol) of the *cis*-$[RuCl_2(dppb)(dphppy)]$ precursor, 14 mg (0.12 mmol) of 2-thiazoline-2-thiol, and 21 mg (0.12 mmol) of KPF_6. Yield: 92 mg (75%). Elem anal. Calcd for $C_{48}H_{46}F_6N_2P_4RuS_2$: C, 63.21; H, 5.42; N, 3.07; S 7.03. Found: C, 63.06; H, 5.35; N, 2.83; S, 6.92. Selected IR (KBr, cm^{-1}): ν(C−H) 3071, 2932, and 2848; ν(C═C) py 1588; ν(C═C) ring phosphine 1482; ν(C═N) py 1449; ν(C═N) 1435; ν(C═C) ϕ 1413; ν(C−S) 1273; β(C−H) ϕ 1159; ν(C−S) 1132; q 1095; ν_{ring} 999; $\nu(PF_6^-)$ 837; γ(C−S) 740; γ(C−H) ϕ 698; ν(P−CH_2) 660; $\nu(PF_6)$ 557; ν(P−C) ϕ 519; y 507; ν(Ru−S) 463; ν(Ru−N) 413. UV/visible spectrum [DMSO; λ_{max}, nm (ε, M^{-1} cm^{-1})]: 262 (30815), 308 (6061), 366 (2207). Molar conductance (S cm^2 mol^{-1}, DMSO): 36.1.

$[Ru(pySm)(dppb)(dphppy)]PF_6$ (Ru2). Compound **Ru2** was synthesized following the general procedure of the synthesis using 100 mg (0.12 mmol) of the *cis*-$[RuCl_2(dppb)(dphppy)]$ precursor, 13 mg (0.12 mmol) of 2-mercaptopyrimidine, and 21 mg (0.12 mmol) of KPF_6. Yield: 108 mg (89%). Elem anal. Calcd for $C_{49}H_{45}F_6N_3P_4RuS$: C, 54.95; H, 4,55; N, 3.90; S, 2.97. Found: C, 54.99; H, 4.43; N, 3.27; S, 2.87. Selected IR (KBr, cm^{-1}): ν(C−H) 3059, 2939, and 2866; ν(C═C) py 1583; ν(C═N)/δ(C−N) 1543; ν(C═C) ring phosphine 1482; ν(C═N) py 1450; ν(C═N) 1433; ν(C−S) 1257; β(C−H) ϕ 1160; ν(C−S) 1136; q 1094; ν_{ring} 1001; $\nu(PF_6)$ 839; γ(C−S) 738; γ(C−H) ϕ 695; ν(P−CH_2) 668; $\nu(PF_6^-)$ 558; ν(P−C) ϕ 519; y 508; ν(Ru−S) 464; ν(Ru−N) 420. UV/visible spectrum [DMSO; λ_{max}, nm (ε, M^{-1} cm^{-1})]: 262 (25185), 306 (8456), 356 (shoulder). Molar conductance (S cm^2 mol^{-1}, DMSO): 33.9.

$[Ru(damp)(dppb)(dphppy)]PF_6$ (Ru3). Compound **Ru3** was synthesized following the general procedure of the synthesis using 100 mg (0.12 mmol) of the *cis*-$[RuCl_2(dppb)(dphppy)]$ precursor, 16 mg (0.12 mmol) of 4,6-diamino-2-mercaptopyridine, and 21 mg (0.12 mmol) of KPF_6. Yield: 99 mg (79%). Elem anal. Calcd for $C_{49}H_{47}F_6N_5P_4RuS \cdot {}^4/_3CH_2Cl_2$: C, 52.39; H, 4.29; N, 6.14; S, 2.81. Found: C, 52.48; H, 4.57; N, 5.71; S, 2.68. Selected IR (KBr, cm^{-1}): ν(N−H) NH_2 3503−3200; ν(C−H) 3059, 2932, and 2856; δ(N−H) NH_2 1543; ν(C═C) py 1584; ν(C═N)/δ(C−N) 1535; ν(C═C) ring phosphine 1474; ν(C═N) py 1448; ν(C═N) 1433; ν(C═C) ϕ 1409; δ(N−H) and ν(C═C) 1321; ν(C−S) 1253; β(C−H) ϕ 1160; ν(C−S) 1130; q 1091; ν_{ring} 999; $\nu(PF_6)$ 847; γ(C−S) 744; γ(C−H) ϕ 700; ν(P−CH_2) 656; $\nu(PF_6^-)$ 558; ν(P−C) ϕ 519; y 507; ν(Ru−S) 462; ν(Ru−N) 424. UV/visible spectrum [DMSO; λ_{max}, nm (ε, M^{-1} cm^{-1})]: 262 (30982), 306 (9087), 368 (2296). Molar conductance (S cm^2 mol^{-1}, DMSO): 35.4.

DNA Interaction Studies. The solution of CT DNA was prepared in a Tris-HCl buffer (5 mM Tris-HCl and 50 mM NaCl, pH 7.4). All solutions of the complexes used in the experiments were prepared in a Tris-HCl buffer containing 10−15% DMSO.

Viscosity Measurements. The viscosity assays were carried out using an Ostwald viscometer maintained at a constant temperature of 298.0 ± 0.3 K in a thermostatic bath. The complex−DNA solutions (4 mL) at different molar ratios, [complex]/[CT DNA] = 0.05, 0.10, 0.15, 0.20, 0.25, and 0.30, were freshly prepared in a Tris-HCl buffer (15% DMSO) prior to use. The DNA concentration in the Tris-HCl buffer was kept constant (200 μM) in all samples. The flow times of the solutions on the Ostwald viscometer were measured at least 6 times using a digital stopwatch and using the mean value. The relative viscosity of DNA in the absence (η_0) and presence (η) of complexes was calculated from eq 1:

$$\eta/\eta_0 = (t - t_0)/(t_{DNA} - t_0) \quad (1)$$

where t_0 and t_{DNA} are the flow times of the buffer and DNA solution alone, respectively, while t is the flow time of the DNA solution in the

https://dx.doi.org/10.1021/acs.inorgchem.0c01835
Inorg. Chem. XXXX, XXX, XXX−XXX

presence of ruthenium compounds.[68] Data are presented as $(\eta/\eta_0)^{1/3}$ versus the ratio [complex]/[DNA].

Agarose Gel Electrophoresis Studies. pBR322 plasmid DNA solutions in a Tris-HCl buffer (10% DMSO) containing 0.0 (control), 0.25, 0.5, and 1.0 equiv of the complexes were incubated for 18 h at 310 K. The plasmid DNA concentration in the Tris-HCl buffer was kept constant (50 μM) in all samples. After incubation, 10 μL of each sample was electrophoresed in agarose gel (1% TAE buffer) for 6 h at 60 V using a Bio-Rad horizontal tank connected to a Consort EV231 variable-potential-power supply. The gels were stained in an ethidium bromide solution (2 μg L^{-1}) and photographed using a ChemiDoc MP imager.

Competitive Displacement Assay with Hoechst 33258. Samples containing CT DNA (100 μM) and Hoechst (2.5 μM) were prepared in a Tris-HCl buffer. Then, the samples (10% DMSO) were treated with amounts of the complexes equivalent to those of Hoechst. The complex/Hoechst DNA ratios were 0, 0.1, 0.2, 0.3, 0.4, 0.5, and 0.6. The fluorescence emission spectra were recorded from 370 to 700 nm at an excitation wavelength of 343 nm using opaque 96-well plates containing 200 μL of solution.

Human Topoisomerase I Inhibition Assay. A human Top IB relaxation kit was purchased from Inspiralis Limited. Reaction mixtures (30 μL) containing 10 mM Tris-HCl (pH 7.9), 50 mM NaCl, 50 mM KCl, 5.0 mM $MgCl_2$, 0.1 mM ethylenediaminetetraacetic acid disodium salt, 15 mg mL^{-1} bovine serum albumin, 1.0 mM adenosine triphosphate, 50 ng pBR322 DNA, and 4.0 nM Topo I containing 0.0 (control), 0.25, and 1.0 equiv of the complexes were incubated for 1 h at 310 K. The reaction was finished by adding 3 μL of sodium lauryl sulfate, and the solution was then incubated again at 333 K for 2 min. After incubation, 15 μL of STEB and 60 μL of a chloroform/isoamyl alcohol (24:1, v/v) mixture were added, and the solution was centrifuged. The aqueous fraction of the samples was collected and analyzed. The samples were electrophoresed in agarose gel (1% TAE buffer) for 12 h at 20 mA using a Bio-Rad horizontal tank connected to a Consort EV231 variable-potential-power supply. The gels were stained in an ethidium bromide solution (2 μg L^{-1}), photographed using a Gel Doc EZ System, and analyzed by an EZ Gel Bio-Rad.

HSA Fluorescence Quenching Experiments. HSA solutions in a Tris-HCl buffer (5% DMSO) containing 0.0 (control), 1, 2, 3, 4, 5, 6, and 7 equiv of the complexes were freshly prepared prior to use. The HSA concentration in the Tris-HCl buffer was kept constant (5 μM) in all samples. The fluorescence emission spectra were recorded from 300 to 500 nm, applying an excitation wavelength of 270 nm. The fluorescence measurements were registered on a SpectraMax M3 at different temperatures (25 and 310 K) in triplicate using an opaque 96-well plate containing 200 μL of solution. The Stern−Volmer quenching constant, bimolecular quenching rate constant, binding constant, and number of binding sites (n) were calculated from the Stern−Volmer and Scatchard equations.[63,65] The thermodynamic parameters (ΔH and ΔS) were determined from the van't Hoff equation: $\ln K = -\Delta H/RT + \Delta S/R$.[53] The change in the free energy (ΔG) was calculated from the equation $\Delta G = -RT \ln K = \Delta H - T\Delta S$.[65]

Proteasome Inhibition in HEK293T-uGFP Cells. A HEK293T cell line stably expressing an unstable version of GFP (uGFP)[78] was cultured at 310 K/5% CO_2 of humid atmosphere. For proteasome inhibition assay, cells were treated with 10 μM MG132 (Boston Biochem) as the positive control or complexes **Ru1**−**Ru3** in the respective concentrations 1, 0.9, and 3.5 μM. After treatment, cells were washed with phosphate-buffered saline (PBS) one time (1×) and harvested with PBS/EDTA 10 mM. Cellular pellets were obtained by centrifugation at 1000g/5 min/277 K and resuspended in PBS (1×) /paraformaldehyde (1%) for 15 min in room temperature. Afterward, cells were centrifuged at 1000g/5 min/277 K, then washed with PBS (1×), and centrifuged in the same conditions. Finally, cellular pellets were resuspended in 10 μg mL^{-1} PI (Thermo), and quantifications were performed by a flow cytometer using a fluorescein isothiocyanate filter (BD Accuri).

In Vitro Proteasome 20S Inhibition. In vitro proteasome inhibition was performed by using 1 μg of a 20S proteasome subunit (Boston Biochem) diluted in 50 mM 4-(2-hydroxyethyl)-1-piperazineethanesulfonic acid (pH 7.6), 100 mM NaCl, and 1 mM dithiothreitol. The purified 20S proteasome was incubated with MG132 or ruthenium(II) complexes for 150 min at 310 K. Following that, proteasome substrate (Suc-LLVY-AMC; Boston Biochem) was added to each reaction at a final concentration of 200 μM. Fluorescence of the succinate group cleaved by proteasome was detected by SpectraMax i3 (Molecular Devices) at λ_{ex} = 380 nm and λ_{em} = 460 nm.

Statistical Analyses. Statistical analyses were performed with a Prism 5 (GraphPad, USA) using the ANOVA one-way test and Tukey's Multiple Comparison Test, considering statistical significance when (*) $p \leq 0.05$, (**) $p < 0.01$, (***)$p < 0.001$, and (****) $p < 0.0001$.

Distribution Coefficient (log *D*). The water/octanol partition coefficients, $P = [\text{compound}]_{n\text{-octanol}}/[\text{compound}]_{\text{water}}$, of the complexes were determined using the shake-flask method.[88] The complexes were added to a mixture of equal volumes of water (750 μL) and n-octanol (750 μL) containing 5% DMSO and were continuously shaken at 310 K for 18 h at 1200 rpm. Measurements of both phases were spectrophotometrically carried out, and the concentrations of the complexes were determined by UV/visible calibration curves in the respective solvents.

In Vitro Assays. *Cell Lines and Culture.* The human triple-negative breast tumor cell line MDA-MB-231 (ATCC HTB-26), the human breast nontumor cell line MCF-10A (ATCC CRL-10317), the human lung tumor cell line A549 (ATCC CCL-185), and the human lung nontumor cell line MRC-5 (ATCC CCL-171) were used. MCF-10A cells were cultured in Dulbecco's modified Eagle medium F12 (DMEM/F12) supplemented with 10% horse serum, 20 ng mL^{-1} epidermal growth factor (EGF), 0.5 μg mL^{-1} hydrocortisone, and 0.01 μg mL^{-1} insulin. A549, MRC-5, and MDA-MB-231 cells were routinely maintained in DMEM/F12 supplemented with 5% fetal bovine serum. All cell lines were maintained at 310 K in an incubator with a humidified 5% CO_2 atmosphere, and 1% penicillin/streptomycin was added to each culture medium.

3-(4,5-Dimethylthiazol-2-yl)-2,5-diphenyltetrazolium Bromide (MTT) Assay. In vitro cytotoxicity of the ruthenium complexes on cell lines was evaluated by MTT assay.[89] Cells (1.5×10^4 cells $well^{-1}$) were seeded in 96-well plates and allowed to adhere for 24 h. Thus, aliquots of complex solutions in DMSO (0.75 μL) were added in different concentrations to each well (containing 150 μL of the medium), which were then incubated for 48 h. DMSO was used as the control on untreated cells (0.5%). After 48 h, 50 μL of MTT (1 mg mL^{-1}) was added to each well. Cells were incubated again for 4 h, the medium was removed, and formazan crystals were solubilized isopropyl alcohol. The absorbance was measured on a microplate spectrophotometer at a wavelength of 540 nm. The cell viability was determined using *GraphPad Prism* software.

Morphology. Morphological assay was performed using the A549 tumor cell line. Cells (0.5×10^5 cells $well^{-1}$) were seeded in a 24-well plate and after 24 h were exposed to different concentrations of complex **Ru2** for an additional 48 h. Cells were examined at times of 0, 24, and 48 h under an inverted optical microscope (NIKON ECLIPSE TS100) with a 10 × objective lens, coupled with a Motcam 1SP camera. The morphological changes of the cells exposed to the treatment were compared to those of the control cells.

Cell Migration Assay. Wound-healing assay was performed to evaluate the effects of the complex on A549 cell migration. Cells (1.0×10^5 cells $well^{-1}$) were seeded in a 12-well plate, and after 24 h, a wound was made in the central portion of every well using a 1 mL sterile tip and washed with PBS to remove unbound cells. Cells were exposed to different concentrations of complex **Ru2** and incubated for 48 h. The region of the wound was examined at times of 0, 24, and 48 h under an inverted optical microscope (NIKON ECLIPSE TS100) with a 4× objective lens, coupled with a Motcam 1SP camera. The closure area (A) of the migrating cells was measured using *ImageJ* software, and the percentage of wound closure was calculated using

https://dx.doi.org/10.1021/acs.inorgchem.0c01835
Inorg. Chem. XXXX, XXX, XXX−XXX

the following equation: % wound closure = $[(A_{0\,h} - A_{24\,h})/A_{0\,h}] \times 100$.

Cell Cycle Measurement. A549 cells (0.5×10^5 cells well^{-1}) were seeded in a 12-well plate and cultured at 310 K for 24 h. After adhesion to the plate, the cells were incubated for another 18 h in a medium supplemented with 2% *N*-succinimidyl 4-fluorobenzoate (SFB) for cell synchronization. Then, the medium was changed to the medium supplemented with 10% SFB, and the cells were treated with different concentrations of the complex for 48 h. Subsequently, the cells were washed with PBS and fixed with ethanol for 24 h at 253 K and again incubated with RNase (0.2 mg mL^{-1}) for 30 min at 310 K. Last, they were incubated with PI (20 μg mL^{-1}) for 1 h on ice and in the dark. The DNA contents were quantified by flow cytometry on an Accuri C6 flow cytometer (BD Biosciences). DMSO (0.5%) was used as the negative control.

Apoptosis Assay. The programmed cell death was evaluated by flow cytometry using an annexin-V-PE Apoptosis Detection Kit (BC Biosciences). A549 cells (0.5×10^5 cells well^{-1}) were seeded in a 12-well plate and cultured at 310 K for 24 h. After adhesion to the plate, the cells were treated with different concentrations of the complex for 48 h. Subsequently, the cells were incubated in the dark with 2.5 μL of annexin-V-PE and 2.5 μL of 7-AAD for 15 min. Cell samples were analyzed in an Accuri C6 flow cytometer (BD Biosciences). Emitted fluorescence by each dye was quantified in *CellQuest* software (BD Biosciences). Camptothecin at 32 μM and DMSO (0.5%) were used like positive and negative controls, respectively.

ICP-MS Measurements. A549 cells (1.5×10^6 cells) were seeded in a Corning Costar 125 cm^2 flask and allowed to attach ~70% of confluency. The medium was replaced by a new culture medium containing complex **Ru2** (0.5 μM), and the cells were incubated for 24 h at 310 K. A separate flask with a free metal medium was used as the control. After the exposition time, the culture medium was transferred to a precleaned tube and centrifuged (1200 rpm, 5 min) to remove floating cells, and the supernatant was collected for further analysis. Then, the A549 cells were washed in ice-cold ultrapure water and trypsinized, and after centrifugation (1200 rpm, 5 min), the cells were resuspended with cooled ultrapure water (2 mL), pelleted, and stored at 253 K for further analysis. Subsequently, sample digestion was performed according to the literature.[52] The quantifications of the metal content were performed by monitoring the ^{102}Ru signal on an Agilent 7800 ICP-MS spectrometer equipped with a concentric nebulizer and a Scott double-pass spray chamber. A single-element ruthenium standard solution used for ICP-MS calibrations was prepared by diluting 1000 mg L^{-1} ^{102}Ru (Qhemis, São Paulo, Brazil) in a 0.14 M HNO_3 medium (previously purified), as well as rhodium and iridium used as internal standards. The analytical solutions for calibration contained from 0.010 to 200 μg L^{-1} of each analyte, and the internal standards were added at 10.0 μg L^{-1} to analytical calibration solutions, analytical blanks, and samples.

■ ASSOCIATED CONTENT

Supporting Information

The Supporting Information is available free of charge at https://pubs.acs.org/doi/10.1021/acs.inorgchem.0c01835.

Experimental details, characterization of all complexes, and detailed assay procedures (PDF)

Accession Codes

CCDC 2006233−2006235 contain the supplementary crystallographic data for this paper. These data can be obtained free of charge via www.ccdc.cam.ac.uk/data_request/cif, or by emailing data_request@ccdc.cam.ac.uk, or by contacting The Cambridge Crystallographic Data Centre, 12 Union Road, Cambridge CB2 1EZ, UK; fax: +44 1223 336033.

■ AUTHOR INFORMATION

Corresponding Authors

Gabriel H. Ribeiro − *Departamento de Química, Universidade Federal de São Carlos, CEP 13565-905 São Carlos, São Paulo, Brazil;* orcid.org/0000-0003-0738-1638; Email: gabrielhenri10@hotmail.com

Alzir A. Batista − *Departamento de Química, Universidade Federal de São Carlos, CEP 13565-905 São Carlos, São Paulo, Brazil;* Email: daab@ufscar.br

Authors

Adriana P. M. Guedes − *Departamento de Química, Universidade Federal de São Carlos, CEP 13565-905 São Carlos, São Paulo, Brazil*

Tamires D. de Oliveira − *Departamento de Química, Universidade Federal de São Carlos, CEP 13565-905 São Carlos, São Paulo, Brazil*

Camila R. S. T. b. de Correia − *Departamento de Genética e Evolução, Universidade Federal de São Carlos, CEP 13565-905 São Carlos, São Paulo, Brazil*

Legna Colina-Vegas − *Departamento de Química, Universidade Federal de São Carlos, CEP 13565-905 São Carlos, São Paulo, Brazil; Instituto de Química, Universidade Federal do Rio Grande do Sul, 91501-970 Porto Alegre, Rio Grande do Sul, Brazil;* orcid.org/0000-0003-3557-5544

Mauro A. Lima − *Departamento de Química, Universidade Federal de São Carlos, CEP 13565-905 São Carlos, São Paulo, Brazil*

Joaquim A. Nóbrega − *Departamento de Química, Universidade Federal de São Carlos, CEP 13565-905 São Carlos, São Paulo, Brazil*

Márcia R. Cominetti − *Departamento de Gerontologia, Universidade Federal de São Carlos, CEP 13565-905 São Carlos, São Paulo, Brazil;* orcid.org/0000-0001-6385-7392

Fillipe V. Rocha − *Departamento de Química, Universidade Federal de São Carlos, CEP 13565-905 São Carlos, São Paulo, Brazil*

Antônio G. Ferreira − *Departamento de Química, Universidade Federal de São Carlos, CEP 13565-905 São Carlos, São Paulo, Brazil*

Eduardo E. Castellano − *Instituto de Física de São Carlos, Universidade de São Paulo, CEP 13560-970 São Carlos, São Paulo, Brazil*

Felipe R. Teixeira − *Departamento de Genética e Evolução, Universidade Federal de São Carlos, CEP 13565-905 São Carlos, São Paulo, Brazil*

Complete contact information is available at: https://pubs.acs.org/10.1021/acs.inorgchem.0c01835

Notes

The authors declare no competing financial interest.

■ ACKNOWLEDGMENTS

The authors gratefully acknowledge the support provided by FAPESP (Grant 2016/16312-0), CNPq, and CAPES. This study was financed, in part, by the Coordenação de Aperfeiçoamento de Pessoal de Nível Superior, Brasil (CAPES), Finance Code 001. L.C.-V. thanks FAPESP for Grant 2016/23130-5.

https://dx.doi.org/10.1021/acs.inorgchem.0c01835
Inorg. Chem. XXXX, XXX, XXX−XXX

REFERENCES

(1) Kenny, R. G.; Marmion, C. J. Toward Multi-Targeted Platinum and Ruthenium Drugs - A New Paradigm in Cancer Drug Treatment Regimens? *Chem. Rev.* **2019**, *119* (2), 1058−1137.

(2) Dasari, S.; Bernard Tchounwou, P. Cisplatin in Cancer Therapy: Molecular Mechanisms of Action. *Eur. J. Pharmacol.* **2014**, *740*, 364−378.

(3) Englinger, B.; Pirker, C.; Heffeter, P.; Terenzi, A.; Kowol, C. R.; Keppler, B. K.; Berger, W. Metal Drugs and the Anticancer Immune Response. *Chem. Rev.* **2019**, *119*, 1519−1624.

(4) Franz, K. J.; Metzler-Nolte, N. Introduction: Metals in Medicine. *Chem. Rev.* **2019**, *119*, 727−729.

(5) Lin, K.; Zhao, Z. Z.; Bo, H.; Hao, X. J.; Wang, J. Q. Applications of Ruthenium Complex in Tumor Diagnosis and Therapy. *Front. Pharmacol.* **2018**, *9*, 1323.

(6) Bacher, F.; Arion, V. B. Ruthenium Compounds as Antitumor Agents: New Developments. *Ref. Modul. Chem. Mol. Sci. Chem. Eng.* **2014**, 1−50.

(7) Thota, S.; Rodrigues, D. A.; Crans, D. C.; Barreiro, E. J. Ru(II) Compounds: Next-Generation Anticancer Metallotherapeutics? *J. Med. Chem.* **2018**, *61*, 5805−5821.

(8) Pal, M.; Nandi, U.; Mukherjee, D. Detailed Account on Activation Mechanisms of Ruthenium Coordination Complexes and Their Role as Antineoplastic Agents. *Eur. J. Med. Chem.* **2018**, *150*, 419−445.

(9) Furrer, J.; Süss-Fink, G. Thiolato-Bridged Dinuclear Arene Ruthenium Complexes and Their Potential as Anticancer Drugs. *Coord. Chem. Rev.* **2016**, *309*, 36−50.

(10) Trondl, R.; Heffeter, P.; Kowol, C. R.; Jakupec, M. A.; Berger, W.; Keppler, B. K. NKP-1339, the First Ruthenium-Based Anticancer Drug on the Edge to Clinical Application. *Chem. Sci.* **2014**, *5*, 2925−2932.

(11) Piccolo, M.; Misso, G.; Ferraro, M. G.; Riccardi, C.; Capuozzo, A.; Zarone, M. R.; Maione, F.; Trifuoggi, M.; Stiuso, P.; D'Errico, G.; Caraglia, M.; Paduano, L.; Montesarchio, D.; Irace, C.; Santamaria, R. Exploring Cellular Uptake, Accumulation and Mechanism of Action of a Cationic Ru-Based Nanosystem in Human Preclinical Models of Breast Cancer. *Sci. Rep.* **2019**, *9*, 1−15.

(12) Alatrash, N.; Issa, F. H.; Bawazir, N. S.; West, S. J.; Van Manen-Brush, K. E.; Shelor, C. P.; Dayoub, A. S.; Myers, K. A.; Janetopoulos, C.; Lewis, E. A.; MacDonnell, F. M. Disruption of Microtubule Function in Cultured Human Cells by a Cytotoxic Ruthenium(Ii) Polypyridyl Complex. *Chem. Sci.* **2020**, *11*, 264−275.

(13) Lv, Z.; Wei, H.; Li, Q.; Su, X.; Liu, S.; Zhang, K. Y.; Lv, W.; Zhao, Q.; Li, X.; Huang, W. Achieving Efficient Photodynamic Therapy under Both Normoxia and Hypoxia Using Cyclometalated Ru(II) Photosensitizer through Type i Photochemical Process. *Chem. Sci.* **2018**, *9*, 502−512.

(14) Naves, M. A.; Graminha, A. E.; Vegas, L. C.; Luna-Dulcey, L.; Honorato, J.; Menezes, A. C. S.; Batista, A. A.; Cominetti, M. R. Transport of the Ruthenium Complex [Ru(GA)(Dppe) 2]PF 6 into Triple-Negative Breast Cancer Cells Is Facilitated by Transferrin Receptors. *Mol. Pharmaceutics* **2019**, *16*, 1167−1183.

(15) De Grandis, R. A.; Santos, P. W.; de Oliveira, K. M.; Machado, A. R. T.; Aissa, A. F.; Batista, A. A.; Antunes, L. M. G.; Pavan, F. R. Novel Lawsone-Containing Ruthenium(II) Complexes: Synthesis, Characterization and Anticancer Activity on 2D and 3D Spheroid Models of Prostate Cancer Cells. *Bioorg. Chem.* **2019**, *85*, 455−468.

(16) Ribeiro, G. H.; Colina-Vegas, L.; Clavijo, J. C. T.; Ellena, J.; Cominetti, M. R.; Batista, A. A. Ru(II)/N-N/PPh3 Complexes as Potential Anticancer Agents against MDA-MB-231 Cancer Cells (N-N = diimine or Diamine). *J. Inorg. Biochem.* **2019**, *193*, 70−83.

(17) Cunha, B. N.; Colina-Vegas, L.; Plutín, A. M.; Silveira, R. G.; Honorato, J.; Oliveira, K. M.; Cominetti, M. R.; Ferreira, A. G.; Castellano, E. E.; Batista, A. A. Hydrolysis Reaction Promotes Changes in Coordination Mode of Ru(II)/Acylthiourea Organometallic Complexes with Cytotoxicity against Human Lung Tumor Cell Lines. *J. Inorg. Biochem.* **2018**, *186*, 147−156.

(18) Correa, R. S.; De Oliveira, K. M.; Delolo, F. G.; Alvarez, A.; Mocelo, R.; Plutin, A. M.; Cominetti, M. R.; Castellano, E. E.; Batista, A. A. Ru(II)-Based Complexes with N-(Acyl)-N′,N′-(Disubstituted)-Thiourea Ligands: Synthesis, Characterization, BSA- and DNA-Binding Studies of New Cytotoxic Agents against Lung and Prostate Tumour Cells. *J. Inorg. Biochem.* **2015**, *150* (Ii), 63−71.

(19) Neves, S. P.; de Carvalho, N. C.; da Silva, M. M.; Rodrigues, A. C. B. C.; Bomfim, L. M.; Dias, R. B.; Sales, C. B. S.; Rocha, C. A. G.; Soares, M. B. P.; Batista, A. A.; Bezerra, D. P. Ruthenium Complexes Containing Heterocyclic Thioamidates Trigger Caspase-Mediated Apoptosis Through MAPK Signaling in Human Hepatocellular Carcinoma Cells. *Front. Oncol.* **2019**, *9*, 562−580.

(20) Takarada, J. E.; Guedes, A. P. M.; Correa, R. S.; Silveira-Lacerda, E. de P.; Castelli, S.; Iacovelli, F.; Deflon, V. M.; Batista, A. A.; Desideri, A. Ru/Fe Bimetallic Complexes: Synthesis, Characterization, Cytotoxicity and Study of Their Interactions with DNA/HSA and Human Topoisomerase IB. *Arch. Biochem. Biophys.* **2017**, *636*, 28−41.

(21) Pires, W. C.; Lima, B. A. V.; de Castro Pereira, F.; Lima, A. P.; Mello-Andrade, F.; Silva, H. D.; da Silva, M. M.; Colina-Vegas, L.; Ellena, J.; Batista, A. A.; de Paul Silveira-Lacerda, E. Ru(II)/Diphenylphosphine/Pyridine-6-Thiolate Complexes Induce S-180 Cell Apoptosis through Intrinsic Mitochondrial Pathway Involving Inhibition of Bcl-2 and P53/Bax Activation. *Mol. Cell. Biochem.* **2018**, *438*, 199−217.

(22) Corrêa, R. S.; Da Silva, M. M.; Graminha, A. E.; Meira, C. S.; dos Santos, J. A. F.; Moreira, D. R. M.; Soares, M. B. P.; Von Poelhsitz, G.; Castellano, E. E.; Bloch, C.; Cominetti, M. R.; Batista, A. A. Ruthenium(II) Complexes of 1,3-Thiazolidine-2-Thione: Cytotoxicity against Tumor Cells and Anti-Trypanosoma Cruzi Activity Enhanced upon Combination with Benznidazole. *J. Inorg. Biochem.* **2016**, *156*, 153−163.

(23) Guedes, A. P. M.; Mello-Andrade, F.; Pires, W. C.; de Sousa, M. A. M.; da Silva, P. F. F.; de Camargo, M. S.; Gemeiner, H.; Amauri, M. A.; Gomes Cardoso, C.; de Melo Reis, P. R.; Silveira-Lacerda, E. de P.; Batista, A. A. Heterobimetallic Ru(II)/Fe(II) Complexes as Potent Anticancer Agents against Breast Cancer Cells, Inducing Apoptosis through Multiple Targets. *Metallomics* **2020**, *12*, 547.

(24) Appelt, P.; da Silva, J. P.; Fuganti, O.; Aquino, L. E. N.; Sandrino, B.; Wohnrath, K.; Santos, V. A. Q.; Cunha, M. A. A.; Veiga, A.; Murakami, F. S.; Back, D. F.; de Araujo, M. P. New Heterobimetallic Ruthenium (II) Complexes [Ru(N-S)(bipy)-(dppf)]PF6: Synthesis, Molecular Structure, Electrochemistry, DFT, Antioxidant and Antibacterial Potential. *J. Organomet. Chem.* **2017**, *846*, 326−334.

(25) Da Silva, M. M.; De Camargo, M. S.; Correa, R. S.; Castelli, S.; De Grandis, R. A.; Takarada, J. E.; Varanda, E. A.; Castellano, E. E.; Deflon, V. M.; Cominetti, M. R.; Desideri, A.; Batista, A. A. Non-Mutagenic Ru(II) Complexes: Cytotoxicity, Topoisomerase IB Inhibition, DNA and HSA Binding. *Dalt. Trans.* **2019**, *48*, 14885−14897.

(26) Velozo-Sá, V. S.; Pereira, L. R.; Lima, A. P.; Mello-Andrade, F.; Rezende, M. R. M.; Goveia, R. M.; Pires, W. C.; Silva, M. M.; Oliveira, K. M.; Ferreira, A. G.; Ellena, J.; Deflon, V. M.; Grisolia, C. K.; Batista, A. A.; Silveira-Lacerda, E. P. In Vitro Cytotoxicity and in Vivo Zebrafish Toxicity Evaluation of Ru(II)/2-Mercaptopyrimidine Complexes. *Dalton Trans.* **2019**, *48*, 6026−6039.

(27) Maggini, S. Classification of P,N-Binucleating Ligands for Hetero- and Homobimetallic Complexes. *Coord. Chem. Rev.* **2009**, *253*, 1793−1832.

(28) Wajda-Hermanowicz, K.; Ciunik, Z.; Kochel, A. Syntheses and Molecular Structure of Some Rh and Ru Complexes with the Chelating Diphenyl (2-Pyridyl)Phosphine Ligand. *Inorg. Chem.* **2006**, *45*, 3369−3377.

(29) Zhang, Z.-Z.; Cheng, H. Chemistry of 2-(Diphenylphosphino)-Pyridine. *Coord. Chem. Rev.* **1996**, *147*, 1−39.

(30) Olmstead, M. M.; Maisonhat, A.; Farr, J. P.; Balch, A. L. Chelating 2-(Diphenylphosphino)Pyridine. *Inorg. Chem.* **1981**, *20*, 4060−4064.

https://dx.doi.org/10.1021/acs.inorgchem.0c01835
Inorg. Chem. XXXX, XXX, XXX−XXX

(31) Agonigi, G.; Riedel, T.; Zacchini, S.; Păunescu, E.; Pampaloni, G.; Bartalucci, N.; Dyson, P. J.; Marchetti, F. Synthesis and Antiproliferative Activity of New Ruthenium Complexes with Ethacrynic-Acid-Modified Pyridine and Triphenylphosphine Ligands. *Inorg. Chem.* **2015**, *54*, 6504−6512.
(32) El-khateeb, M.; Damer, K.; Görls, H.; Weigand, W. Pyridine- and Pyrimidine-2-Thiolate Complexes of Ruthenium. *J. Organomet. Chem.* **2007**, *692*, 2227−2233.
(33) Bomfim, L. M.; de Araujo, F. A.; Dias, R. B.; Sales, C. B. S.; Rocha, C. A. G.; Correa, R. S.; Soares, M. B. P.; Batista, A. A.; Bezerra, D. P. Ruthenium(II) Complexes with 6-Methyl-2-Thiouracil Selectively Reduce Cell Proliferation, Cause DNA Double-Strand Break and Trigger Caspase-Mediated Apoptosis through JNK/P38 Pathways in Human Acute Promyelocytic Leukemia Cells. *Sci. Rep.* **2019**, *9*, 11483−11500.
(34) Biancalana, L.; Pratesi, A.; Chiellini, F.; Zacchini, S.; Funaioli, T.; Gabbiani, C.; Marchetti, F. Ruthenium Arene Complexes with Triphenylphosphane Ligands: Cytotoxicity towards Pancreatic Cancer Cells, Interaction with Model Proteins, and Effect of Ethacrynic Acid Substitution. *New J. Chem.* **2017**, *41*, 14574−14588.
(35) Sáez, R.; Lorenzo, J.; Prieto, M. J.; Font-Bardia, M.; Calvet, T.; Omeñaca, N.; Vilaseca, M.; Moreno, V. Influence of PPh3Moiety in the Anticancer Activity of New Organometallic Ruthenium Complexes. *J. Inorg. Biochem.* **2014**, *136*, 1−12.
(36) Ciechanover, A. The Ubiquitin-Proteasome Proteolytic Pathway. *Cell* **1994**, *79*, 13−21.
(37) Manasanch, E. E.; Orlowski, R. Z. Proteasome Inhibitors in Cancer Therapy. *Nat. Rev. Clin. Oncol.* **2017**, *14*, 417−433.
(38) Bianchi, G.; Oliva, L.; Cascio, P.; Pengo, N.; Fontana, F.; Cerruti, F.; Orsi, A.; Pasqualetto, E.; Mezghrani, A.; Calbi, V.; Palladini, G.; Giuliani, N.; Anderson, K. C.; Sitia, R.; Cenci, S. The Proteasome Load versus Capacity Balance Determines Apoptotic Sensitivity of Multiple Myeloma Cells to Proteasome Inhibition. *Blood* **2009**, *113*, 3040−3049.
(39) Rastogi, N.; Mishra, D. P. Therapeutic Targeting of Cancer Cell Cycle Using Proteasome Inhibitors. *Cell Div.* **2012**, *7*, 26.
(40) Siu, F. M.; Lin, I. W. S.; Yan, K.; Lok, C. N.; Low, K. H.; Leung, T. Y. C.; Lam, T. L.; Che, C. M. Anticancer Dirhodium(Ii,Ii) Carboxylates as Potent Inhibitors of Ubiquitin-Proteasome System. *Chem. Sci.* **2012**, *3*, 1785−1793.
(41) Tong, M.; Smeekens, J. M.; Xiao, H.; Wu, R. Systematic Quantification of the Dynamics of Newly Synthesized Proteins Unveiling Their Degradation Pathways in Human Cells. *Chem. Sci.* **2020**, *11*, 3557−3568.
(42) Chen, D.; Frezza, M.; Schmitt, S.; Kanwar, J.; Dou, Q. Bortezomib as the First Proteasome Inhibitor Anticancer Drug: Current Status and Future Perspectives. *Curr. Cancer Drug Targets* **2011**, *11*, 239−253.
(43) Essoun, E.; Wang, R.; Aquino, M. A. S. Disassembly of Diruthenium(II,III) Tetraacetate with P−N Donor Ligands. *Inorg. Chim. Acta* **2017**, *454*, 97−106.
(44) Kumar, P.; Singh, A. K.; Yadav, M.; Li, P. Z.; Singh, S. K.; Xu, Q.; Pandey, D. S. Synthesis and Characterization of Ruthenium(II) Complexes Based on Diphenyl-2-Pyridylphosphine and Their Applications in Transfer Hydrogenation of Ketones. *Inorg. Chim. Acta* **2011**, *368*, 124−131.
(45) Kumar, P.; Yadav, M.; Singh, A. K.; Pandey, D. S. Synthesis and Characterization of Some Novel Ruthenium(II) Complexes Containing Thiolate Ligands. *J. Organomet. Chem.* **2010**, *695*, 994−1001.
(46) Gilli, G.; Gilli, P. *The Nature of the Hydrogen Bond: Outline of a Comprehensive Hydrogen Bond Theory*; Oxford University Press: New York, 2009; DOI: 10.1093/acprof:oso/9780199558964.001.0001.
(47) He, M.; Du, F.; Zhang, W. Y.; Yi, Q. Y.; Wang, Y. J.; Yin, H.; Bai, L.; Gu, Y. Y.; Liu, Y. J. Photoinduced Anticancer Effect Evaluation of Ruthenium(II) Polypyridyl Complexes toward Human Lung Cancer A549 Cells. *Polyhedron* **2019**, *165*, 97−110.
(48) Peña, B.; Saha, S.; Barhoumi, R.; Burghardt, R. C.; Dunbar, K. R. Ruthenium(II)-Polypyridyl Compounds with π-Extended Nitrogen Donor Ligands Induce Apoptosis in Human Lung Adenocarcinoma (A549) Cells by Triggering Caspase-3/7 Pathway. *Inorg. Chem.* **2018**, *57*, 12777−12786.
(49) Sun, D.; Mou, Z.; Li, N.; Zhang, W.; Wang, Y.; Yang, E.; Wang, W. Anti-Tumor Activity and Mechanism of Apoptosis of A549 Induced by Ruthenium Complex. *JBIC, J. Biol. Inorg. Chem.* **2016**, *21*, 945−956.
(50) Qasim Warraich, M.; Ghion, A.; Perdisatt, L.; O'Neill, L.; Casey, A.; O'Connor, C. In Vitro Cytotoxicity, Cellular Uptake, Reactive Oxygen Species and Cell Cycle Arrest Studies of Novel Ruthenium(II) Polypyridyl Complexes towards A549 Lung Cancer Cell Line. *Drug Chem. Toxicol.* **2019**, *0*, 1−11.
(51) Babak, M. V.; Meier, S. M.; Huber, K. V. M.; Reynisson, J.; Legin, A. A.; Jakupec, M. A.; Roller, A.; Stukalov, A.; Gridling, M.; Bennett, K. L.; Colinge, J.; Berger, W.; Dyson, P. J.; Superti-Furga, G.; Keppler, B. K.; Hartinger, C. G. Target Profiling of an Antimetastatic RAPTA Agent by Chemical Proteomics: Relevance to the Mode of Action. *Chem. Sci.* **2015**, *6*, 2449−2456.
(52) Lenis-Rojas, O. A.; Robalo, M. P.; Tomaz, A. I.; Carvalho, A.; Fernandes, A. R.; Marques, F.; Folgueira, M.; Yánez, J.; Vázquez-García, D.; López Torres, M.; Fernández, A.; Fernández, J. J. RuII(p-Cymene) Compounds as Effective and Selective Anticancer Candidates with No Toxicity in Vivo. *Inorg. Chem.* **2018**, *57*, 13150−13166.
(53) Swaminathan, S.; Haribabu, J.; Kalagatur, N. K.; Konakanchi, R.; Balakrishnan, N.; Bhuvanesh, N.; Karvembu, R. Synthesis and Anticancer Activity of [RuCl2(H6-Arene)(Aroylthiourea)] Complexes—High Activity against the Human Neuroblastoma (IMR-32) Cancer Cell Line. *ACS Omega* **2019**, *4*, 6245−6256.
(54) Pantić, D. N.; Mihajlović-lalić, L. E.; Aranđelović, S.; Radulović, S.; Grgurić-šipka, S. Synthesis, Characterization and Cytotoxic Activity of Organoruthenium (II) -Halido Complexes with 5-Chloro-1 H -Benzimidazole-2-Carboxylic Acid. *J. Coord. Chem.* **2019**, *72*, 908−919.
(55) Muralisankar, M.; Dheepika, R.; Haribabu, J.; Balachandran, C.; Aoki, S.; Bhuvanesh, N. S. P.; Nagarajan, S. Design, Synthesis, DNA/HSA Binding, and Cytotoxic Activity of Half-Sandwich Ru(II)-Arene Complexes Containing Triarylamine−Thiosemicarbazone Hybrids. *ACS Omega* **2019**, *4*, 11712−11723.
(56) Chen, F.; Romero-Canelón, I.; Soldevila-Barreda, J. J.; Song, J.-I.; Coverdale, J. P. C.; Clarkson, G. J.; Kasparkova, J.; Habtemariam, A.; Wills, M.; Brabec, V.; Sadler, P. J. Transfer Hydrogenation and Antiproliferative Activity of Tethered Half-Sandwich Organoruthenium Catalysts. *Organometallics* **2018**, *37* (10), 1555−1566.
(57) Ge, X.; Chen, S.; Liu, X.; Wang, Q.; Gao, L.; Zhao, C.; Zhang, L.; Shao, M.; Yuan, X. A.; Tian, L.; Liu, Z. Ferrocene-Appended Iridium(III) Complexes: Configuration Regulation, Anticancer Application, and Mechanism Research. *Inorg. Chem.* **2019**, *58* (20), 14175−14184.
(58) Ma, W.; Guo, L.; Tian, Z.; Zhang, S.; He, X.; Li, J.; Yang, Y.; Liu, Z. Rhodamine-Modified Fluorescent Half-Sandwich Iridium and Ruthenium Complexes: Potential Application as Bioimaging and Anticancer Agents. *Dalt. Trans.* **2019**, *48* (15), 4788−4793.
(59) Li, J. J.; Tian, Z.; Ge, X.; Xu, Z.; Feng, Y.; Liu, Z. Design, Synthesis, and Evaluation of Fluorine and Naphthyridine−Based Half-Sandwich Organoiridium/Ruthenium Complexes with Bioimaging and Anticancer Activity. *Eur. Eur. J. Med. Chem.* **2019**, *163*, 830−839.
(60) Yamaguchi, H.; Wyckoff, J.; Condeelis, J. Cell Migration in Tumors. *Curr. Opin. Cell Biol.* **2005**, *17*, 559−564.
(61) Gordon, E.; Ravicz, J.; Liu, S.; Chawla, S.; Hall, F. Cell Cycle Checkpoint Control: The Cyclin G1/Mdm2/P53 Axis Emerges as a Strategic Target for Broad-spectrum Cancer Gene Therapy - A Review of Molecular Mechanisms for Oncologists. *Mol. Clin. Oncol.* **2018**, *9*, 115−134.
(62) Pucci, B.; Kasten, M.; Giordano, A. Cell Cycle and Apoptosis 1. *Neoplasia* **2000**, *2*, 291−299.
(63) Naveenraj, S.; Anandan, S. Binding of Serum Albumins with Bioactive Substances − Nanoparticles to Drugs. *J. Photochem. Photobiol., C* **2013**, *14*, 53−71.

https://dx.doi.org/10.1021/acs.inorgchem.0c01835
Inorg. Chem. XXXX, XXX, XXX−XXX

(64) Lee, P.; Wu, X. Review: Modifications of Human Serum Albumin and Their Binding Effect. *Curr. Pharm. Des.* **2015**, *21*, 1862−1865.
(65) Ross, P. D.; Subramanian, S. Thermodynamics of Protein Association Reactions: Forces Contributing to Stability1. *Biochemistry* **1981**, *20*, 3096−3102.
(66) Helms, M. K.; Petersen, C. E.; Bhagavan, N. V.; Jameson, D. M. Time-Resolved Fluorescence Studies on Site-Directed Mutants of Human Serum Albumin. *FEBS Lett.* **1997**, *408*, 67−70.
(67) Rilak Simović, A.; Masnikosa, R.; Bratsos, I.; Alessio, E. Chemistry and Reactivity of Ruthenium(II) Complexes: DNA/Protein Binding Mode and Anticancer Activity Are Related to the Complex Structure. *Coord. Chem. Rev.* **2019**, *398*, 113011−113037.
(68) Scruggs, R. L.; Ross, P. D. Viscosity Study of DNA. *Biopolymers* **1964**, *2*, 593−609.
(69) Rehman, S. U.; Sarwar, T.; Husain, M. A.; Ishqi, H. M.; Tabish, M. Studying Non-Covalent Drug-DNA Interactions. *Arch. Biochem. Biophys.* **2015**, *576*, 49−60.
(70) Stout, D. L.; Becker, F. F. Fluorometric Quantitation of Single-Stranded DNA: A Method Applicable to the Technique of Alkaline Elution. *Anal. Biochem.* **1982**, *127*, 302.
(71) Pages, B. J.; Ang, D. L.; Wright, E. P.; Aldrich-Wright, J. R. Metal Complex Interactions with DNA. *Dalt. Trans.* **2015**, *44*, 3505−3526.
(72) Bjornsti, M. A.; Kaufmann, S. H. Topoisomerases and Cancer Chemotherapy: Recent Advances and Unanswered Questions. *F1000Research* **2019**, *8*, 1704.
(73) Pommier, Y. Diversity of DNA Topoisomerases 1I and Inhibitors DNA Topoisomerase !/Topoisomerase Inhibitors/Cancer Cells DNA Topoisomerase I Diversity. *Biochimie* **1998**, *80*, 255−270.
(74) Stewart, L.; Redinbo, M. R.; Qiu, X.; Hol, W. G. J.; Champoux, J. J. A Model for the Mechanism of Human Topoisomerase I. *Science (Washington, DC, U. S.)* **1998**, *279*, 1534−1541.
(75) Sordet, O.; Khan, Q. A.; Kohn, K. W.; Pommier, Y. Apoptosis Induced by Topoisomerase Inhibitors. *Curr. Med. Chem.: Anti-Cancer Agents* **2003**, *3*, 271−290.
(76) Gaur, R.; Choubey, D. K.; Usman, M.; Ward, B. D.; Roy, J. K.; Mishra, L. Synthesis, Structures, Nuclease Activity, Cytotoxicity, DFT and Molecular Docking Studies of Two Nitrato Bridged Homodinuclear (Cu-Cu, Zn-Zn) Complexes Containing 2,2′-Bipyridine and a Chalcone Derivative. *J. Photochem. Photobiol., B* **2017**, *173*, 650−660.
(77) Gaur, R.; Mishra, L. Synthesis and Characterization of Ru(II)−DMSO−Cl−Chalcone Complexes: DNA Binding, Nuclease, and Topoisomerase II Inhibitory Activity. *Inorg. Chem.* **2012**, *51* (5), 3059−3070.
(78) Dantuma, N. P.; Lindsten, K.; Glas, R.; Jellne, M.; Masucci, M. G. Short-Lived Green Fluorescent Proteins for Quantifying Ubiquitin/Proteasome- Dependent Proteolysis in Living Cells. *Nat. Biotechnol.* **2000**, *18*, 538−543.
(79) Pacifico, S.; Ferretti, V.; Albanese, V.; Fantinati, A.; Gallerani, E.; Nicoli, F.; Gavioli, R.; Zamberlan, F.; Preti, D.; Marastoni, M. Synthesis and Biological Activity of Peptide α-Ketoamide Derivatives as Proteasome Inhibitors. *ACS Med. Chem. Lett.* **2019**, *10*, 1086−1092.
(80) Hooft, R. W. W. *COLLECT Data Collection Software*; Enraf-Nonius BV: Delft, The Netherlands, 1998.
(81) Farrugia, L. J. WinGX and ORTEP for Windows: An Update. *J. Appl. Crystallogr.* **2012**, *45*, 849−854.
(82) Otwinowski, Z.; Minor, W. Processing of X-Ray Diffraction Data Collected in Oscillation Mode. *Methods Enzymol.* **1997**, *276*, 307−326.
(83) Sheldrick, G. M. A Short History of SHELX. *Acta Crystallogr., Sect. A: Found. Crystallogr.* **2008**, *64*, 112−122.
(84) Frisch, M. J.; Trucks, G. W.; Schlegel, H. B.; Scuseria, G. E.; Robb, M. a.; Cheeseman, J. R.; Scalmani, G.; Barone, V.; Petersson, G. a.; Nakatsuji, H.; Cammi, R.; Ochterski, J. W.; Martin, R. L.; Morokuma, K.; Farkas, O.; Foresman, J. B.; Fox *Gaussian 16*, revision C.01; Gaussian, Inc.: Wallingford, CT, 2009.
(85) Stephenson, T. A.; Wilkinson, G. NucL Chem. *J. Inorg. Nucl. Chem.* **1966**, *28*, 945−956.
(86) Jung, C. W.; Garrou, P. E.; Hoffman, P. R.; Caulton, K. G. Reexamination of the Reactions of Ph2P(CH2)NPPh2 (n = 1−4) with RuCl2(PPh3)3. *Inorg. Chem.* **1984**, *23*, 726−729.
(87) Schutte, R. P.; Rettig, S. J.; Joshi, A. M.; James, B. R. Synthesis, Structure, and Reactivity of [RuCl(PP)L]PF6 (PP) = (PPh 3)2, Ph2P(CH2)4PPh2 ; L) P(Py)3, PPh(Py)2, Py) 2-Pyridyl). The "Missing" P,N,N′-Coordination Mode for 2-Pyridylphosphines. *Inorg. Chem.* **1997**, *36*, 5809−5817.
(88) Baka, E.; Comer, J. E. A.; Takács-Novák, K. Study of Equilibrium Solubility Measurement by Saturation Shake-Flask Method Using Hydrochlorothiazide as Model Compound. *J. Pharm. Biomed. Anal.* **2008**, *46*, 335−341.
(89) Mosmann, T. Rapid Colorimetric Assay for Cellular Growth and Survival: Application to Proliferation and Cytotoxicity Assays. *J. Immunol. Methods* **1983**, *65*, 55−63.

https://dx.doi.org/10.1021/acs.inorgchem.0c01835
Inorg. Chem. XXXX, XXX, XXX−XXX